Road Materials and Pavement Design

ISSN: (Print) (Online) Journal homepage: https://www.tandfonline.com/loi/trmp20

Analytical modelling of complex stiffness modulus tests in direct tension-compression on asphalt concrete and nonlinearity effect due to strain amplitude

L. Coulon, G. Koval, C. Chazallon & J.-N. Roux

To cite this article: L. Coulon, G. Koval, C. Chazallon & J.-N. Roux (2023) Analytical modelling of complex stiffness modulus tests in direct tension-compression on asphalt concrete and nonlinearity effect due to strain amplitude, Road Materials and Pavement Design, 24:1, 216-246, DOI: 10.1080/14680629.2021.2014349

To link to this article: https://doi.org/10.1080/14680629.2021.2014349

ROAD MATERIALS AND PAVEMENT DESIGN
2023, VOL. 24, NO. 1, 216–246
https://doi.org/10.1080/14680629.2021.2014349

Taylor & Francis
Taylor & Francis Group

Analytical modelling of complex stiffness modulus tests in direct tension-compression on asphalt concrete and nonlinearity effect due to strain amplitude

L. Coulon[a], G. Koval[a], C. Chazallon[a] and J.-N. Roux[b]

[a]ICube (CNRS UMR 7357), INSA Strasbourg, Strasbourg, France; [b]Laboratoire Navier (CNRS UMR 8205), Université Gustave Eiffel, Marne-la-Vallée, France

ABSTRACT

A new analytical model is designed to reproduce the complex modulus of asphalt concrete in cyclic dynamic tests. Instead of multiplying rheological elements with fixed parameters, only two elements with variable parameters are connected in parallel: the stiffness component $\Re_E$ related to the strain and the viscosity component $\Im_\eta$ related to the strain rate. They compose the VENoL (NOnLinear ViscoElastic) model. Their variations as a function of pulsation are calibrated with the Carreau–Yasuda model at a reference temperature and strain amplitude. The conversion from one temperature to another is done using the Time-Temperature Superposition Principle defined by its shift factor a_T. For the conversion from one strain amplitude to another (nonlinearity), the Time-Amplitude Semi-Superposition Principle is newly created, defined by two shift factors a_A and b_A. The model is calibrated with experimental data from the literature based on direct tension-compression tests. The results obtained corroborate the experiments accurately.

ARTICLE HISTORY
Received 12 March 2021
Accepted 30 November 2021

KEYWORDS
Asphalt concrete; complex modulus; dynamic analysis; nonlinearity; superposition principle; VENoL model

1. Introduction

1.1. Linear and nonlinear viscoelastic regions of asphalt materials in dynamic analysis

A material is defined as Linear ViscoElastic (LVE) if stress is proportional to strain at any given time and if the Boltzmann superposition principle holds. However, like many materials, asphalt materials are NonLinear ViscoElastic (NLVE). Thus, to apply LVE theory, it is important to define the limits of the region for which the material behaviour can still be considered LVE. It is known that the influence of temperature and loading time (frequency) on the relationship between stress and strain belongs to the LVE region. The method of generating master curves using the Time-Temperature Superposition Principle (TTSP) applies within the LVE region and also within the NLVE region (Graziani et al., 2019; Nguyen et al., 2015).

Recently, several scientists attempted to define the range of strain amplitude with cyclic tests for which the asphalt materials could be considered LVE. By analysing strain sweep data for asphalt binders during the SHRP study, Anderson et al. (1994) found that there was rarely a clear distinction between LVE and NLVE regions but that with increasing strain levels, the norm of the complex stiffness modulus decreased at an ever-increasing rate. Therefore, they arbitrarily established the upper limit of

CONTACT L. Coulon leo.coulon@insa-strasbourg.fr

the LVE region as the point at which the modulus decreases to 95% of its initial value. From this criterion, Airey et al. (2004) found that the LVE bulk strain limit for mixtures was in the order of 100 μm/m, in line with the Rilem recommendation (Di Benedetto et al., 2001).

However, this LVE limit should be considered only as an approximation. Indeed, the 95% LVE limit is highly dependent on temperature and frequency conditions (Airey et al., 2004; Babadopulos et al., 2019). Then, several experimental studies on mixtures have shown that the norm of the modulus decreased almost linearly with increasing strains levels both below and above the LVE limit (Doubbaneh, 1995; Phan et al., 2017; Underwood & Kim, 2012; Uzan & Levenberg, 2007). Furthermore, in addition to nonlinearity during strain sweep tests, other effects may develop depending on the strain amplitude level and the number of cycles, such as self-heating, thixotropy and damage (Di Benedetto et al., 2011; Gauthier et al., 2010; Mangiafico et al., 2018; Nguyen et al., 2019). They may lead to erroneous conclusions.

1.2. Modelling the behaviour of asphalt concrete under dynamic loading

1.2.1. Modelling the linear viscoelastic behaviour

For several decades, many scientists have focused on creating rheological models to reproduce the LVE behaviour of asphalt concrete under dynamic loading over a wide range of temperatures (−30 to 50°C) and frequencies (0.001 Hz to 10 Hz). Two categories of rheological models can be distinguished: Discrete Relaxation Spectrum Models (DRSM) and Continuous Relaxation Spectrum Models (CRSM). Among DRSMs, we can list the generalised Maxwell model (or Prony series) and the generalised Kelvin–Voigt model. They can correctly simulate the behaviour of asphalt mixes, but provided that enough elements are used, i.e. at least thirty parameters (Xu & Solaimanian, 2009). CRSMs can be represented by an infinity of Maxwell elements in parallel or Kelvin–Voigt elements in series. They appeared with the use of parabolic elements. The most famous is the 2S2P1D model, composed of two springs, two parabolic elements and one dashpot (Huet, 1963; Olard, 2003; Sayegh, 1965). It gives a correct simulation of the behaviour of asphalt concrete for only seven parameters, plus two defining the TTSP. However, it only approximates the curve return in the Black space at high temperature and low frequency, as we can check from this thesis (Mangiafico, 2014, Figure 4.25).

Other modelling proposals are based on analytical expressions. For example, the CAM model, composed of the initials of its three authors, characterises the behaviour of bitumen binders with two equations expressing the norm of the complex shear modulus as well as the phase angle according to the pulsation (or angular frequency) (Christensen & Anderson, 1992; Marasteanu, 1999). A generalisation of this model to binders and mixtures was also proposed by Zeng et al. (2001) with acceptable results for nine parameters, plus two defining the TTSP.

1.2.2. Modelling the nonlinear viscoelastic behaviour

First, in 1969, Richard Schapery (1969) developed nonlinear viscoelastic constitutive equations for engineering materials in the time domain. He noticed that it was possible to switch from one level of stress (or strain) to another with four coefficients: a_σ (or a_ε), a shift factor to calculate a reduced time, g_0, g_1, and g_2 (or h_e, h_1, and h_2), three nonlinear parameters; all equal to 1.0 when the stress (or strain) is sufficiently small. Menglan Zeng (1997) used this model to analyse the nonlinear behaviour of asphalt concrete in stress relaxation. He obtained good results, but a lot of calibration work was needed. He also defined that the temperature dependency could be added to the model by multiplying the shift factor a_T of the TTSP with the shift factor a_ε.

In cyclic dynamic analysis, Zeng et al. (2001) used this time an analytical approach with the generalised CAM model to reproduce at different strain amplitudes the complex stiffness modulus of binders and mixtures. They created a shift factor a_γ to calculate a reduced frequency. The Williams-Landel-Ferry (WLF) equation (Williams et al., 1955), usually used to define the shift factor a_T of the TTSP, was considered appropriate for expressing variations of a_γ as a function of strain amplitude. However, the simulations obtained for the phase angle were incomplete. A vertical shift factor seems to be missing.

Other researchers tried to improve the 2S2P1D model into a nonlinear model for mixtures. Nguyen et al. (2015) created the 2S2P1Dnl model. As a first approach, they introduced the hypothesis of a linear decrease of the modulus according to the strain amplitude applied to each spring and the group of parabolic elements. The results obtained are correct for the norm of the stiffness modulus, but not for the phase angle. On the other hand, Graziani et al. (2019) calibrated the 2S2P1D model for each complex stiffness modulus obtained at 15, 30 and 60 µm/m. Then, they proposed phenomenological equations about variations of the parameters of the 2S2P1D model according to the strain amplitude. But this process strongly depends on the quality of the fit and the assumptions made. For example, they assumed that the minimum and maximum bounds of the complex stiffness modulus varied with the strain amplitude. However, the nonlinearity fades as it approaches low temperatures and high frequencies (Nguyen et al., 2015).

1.3. Study presented in this paper

The study presented hereafter is a part of a larger research effort within a Ph.D. thesis (Coulon, 2022), itself integrated into the national project ANR MoveDVDC. The objective of this thesis is to numerically reproduce, with the Discrete Element Method (DEM), cyclic tests of complex modulus and fatigue on asphalt concrete. Nevertheless, this paper is only devoted to the first step which defines a rheological model that can be easily implemented as a contact law in DEM and that can reproduce the instantaneous LVE behaviour of asphalt concrete. The addition of the nonlinear behaviour is also essential to make the transition, for example, from a complex modulus test at 50 µm/m to the initial modulus of a fatigue test at 100 µm/m.

The LVE models listed in Section 1.2.1 were not suitable for our purposes. Indeed, the DRSMs require too many parameters to reproduce the complex stiffness modulus at different temperatures and frequencies. The precision of the 2S2P1D model would have been sufficient if it did not need fractional derivatives, which are difficult to implement in numerical simulations. The choice was therefore to create a new analytical model, with a different structure from the CAM model. Indeed, we think that modelling the norm of the complex stiffness modulus and the phase angle is not the right choice since they are calculated from the real and imaginary parts of the modulus. The real part is associated with elasticity and the imaginary part with viscosity. Consequently, their effects are combined within the norm and the phase angle, which complicates the observations, especially if we need to add the effect of nonlinearity.

Regarding the integration of the NLVE behaviour, the nonlinear viscoelastic constitutive equations were not retained because they are too difficult to implement in DEM. The other models listed in section 1.2.2 are imprecise, but the analytical approach developed by Zeng et al. (2001) seemed to be the most promising. This incomplete approach has therefore been improved in this paper. The development of this approach has led to a better understanding of the mechanisms leading to nonlinearity.

We gave to this new model the name 'VENoL model', for NOnLinear ViscoElastic model. It was developed using experimental data from the literature and obtained from complex modulus tests in Direct Tension-Compression (DTC) on cylindrical specimens with a strain control mode. The VENoL model was briefly introduced for the first time in the conference paper (Coulon et al., 2021).

Table 1 gives the meanings of the different acronyms used in the legends of the graphics of this paper.

2. VENoL model design

2.1. General equation

In dynamic analysis, the complex stiffness modulus $E^*(t)$ is obtained by dividing the stress signal $\sigma^*(t)$ by the strain signal $\varepsilon^*(t)$ (Equations (1)–(3)). ε_0 is the strain amplitude, σ_0, the stress amplitude and φ,

Table 1. Meaning of acronyms in the legends of the graphics.

Acronym	Meaning
CMT	Complex Modulus Test
NLT	NonLinearity Test
SART	Strain Amplitude Rise Test
Exp	Experiment
Mod	Modelling
20/10	Test conditions 20°C/10 Hz

the phase angle.

$$\sigma^*(t) = E^*(t) \cdot \varepsilon^*(t) \tag{1}$$

where,

$$\varepsilon^*(t) = \varepsilon_0 \cdot e^{j\cdot\omega t} \tag{2}$$

$$\sigma^*(t) = \sigma_0 \cdot e^{j\cdot(\omega t+\varphi)} \tag{3}$$

The stiffness modulus can split its complex form into two, composed of a real part $\Re(E^*)$ and an imaginary part $\Im(E^*)$ having the units Pascal (Equation (4)). By dividing $\Im(E^*)$ by the signal pulsation ω, we obtain $\Im_\eta$ akin to a viscosity (Equation (5)). We call it the 'viscosity component'. The choice of its symbol refers to the imaginary part of E^* and the viscosity, because $\Im_\eta$ is also the real part of the complex viscosity modulus η^*. In the same way, we replace $\Re(E^*)$ by $\Re_E$ and we call it the 'stiffness component' (Equation (5)). The choice of its symbol reminds us that it is related to the real part of E^* and the elasticity. The multiplication of $i\omega$ by $\varepsilon^*(t)$ gives the derived function, the strain rate $\dot{\varepsilon}^*(t)$. Therefore, the general equation is naturally obtained (Equation (6)).

$$\sigma^*(t) = [\Re(E^*) + i \cdot \Im(E^*)] \cdot \varepsilon^*(t) \tag{4}$$

$$\sigma^*(t) = [\Re_E + i\omega \cdot \Im_\eta] \cdot \varepsilon^*(t) \tag{5}$$

$$\text{where, } \begin{cases} \Re(E^*) = \Re_E \\ \Im(E^*) = \omega \cdot \Im_\eta \end{cases}$$

$$\sigma^*(t) = \Re_E \cdot \varepsilon^*(t) + \Im_\eta \cdot \dot{\varepsilon}^*(t) \tag{6}$$

2.2. Representation

This general Equation (6) is similar to that of the Kelvin–Voigt model composed in parallel of a spring of elasticity E and a dashpot of viscosity η. By analogy, the VENoL model can therefore be schematically represented with two elements $\Re_E$ and $\Im_\eta$ connected in parallel (Figure 1). Thus, with only two elements, the VENoL model can be easily implemented as a contact law in numerical simulations using the Discrete Element Method.

2.3. Variation of stiffness and viscosity components

The stiffness component $\Re_E$ and the viscosity component $\Im_\eta$ can vary according to entry conditions: temperature T of the environment, pulsation ω and strain amplitude ε_0 of the imposed signal. These three parameters influence the viscoelasticity of asphalt concrete. Their effects are integrated into the VENoL model in the following sections.

- In Section 3, the LVE behaviour is added to the VENoL model. Variations of the components $\Re_E$ and $\Im_\eta$ as a function of pulsation are fitted using mathematical functions at a reference temperature.

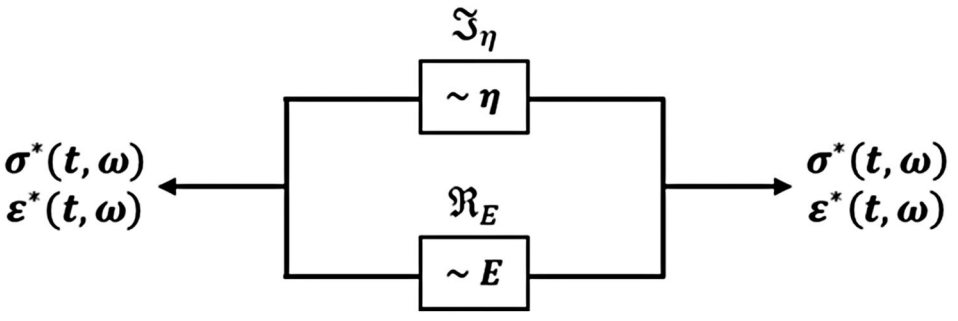

Figure 1. Schematic diagram of the VENoL model.

The temperature effect can be added with a shift factor a_T from the Time-Temperature Superposition Principle. To set up this point, experimental data from Mangiafico (2014) and obtained with DTC tests on one cylindrical specimen in strain control mode are used.

- In Section 4, the NLVE behaviour is added to the VENoL model. A new principle is developed: the Time-Amplitude Semi-Superposition Principle. It takes into account the influence of the strain amplitude on the components $\Re_E$ and $\Im_\eta$ by means of two shift factors a_A and b_A. To set up this point, experimental data from Graziani et al. (2019) are used. These data were obtained with DTC tests on two cylindrical specimens at three different strain amplitudes: 15, 30 and 60 µm/m. Thus, the study of nonlinearity is carried out at small amplitudes.

3. Building the VENoL model: considering the influence of temperature and pulsation

3.1. Use of Mangiafico's experimental data

To implement the temperature and pulsation effects in the VENoL model, Mangiafico's experimental data, from DTC tests on asphalt concrete and published in 2014 in his thesis, are used (Mangiafico, 2014).

3.1.1. Summary description of the specimen analysed

In his thesis, Salvatore Mangiafico launched a significant Campaign A whose objective was to evaluate the influence of Reclaimed Asphalt Pavement (RAP) material on the mechanical properties of bituminous mixtures. A total of twenty-one different mixtures were produced and tested in Campaign A, with different RAP material contents and binder types. For this paper, only the results of one control mixture are used. This material was a high modulus asphalt mixture ('Enrobé à Module Élevé' in French) respecting European standard (NF EN 13108-1, February 2007). It was produced with a fresh binder of penetration grade 35/50 and dosed at 5.35% by weight of the final mix. The mixture was characterised by a continuous grading curve of 0/14 mm made of silica-limestone aggregates. As it was a control mixture, it contained 0% of RAP. Hence the mixture reference name A.0.35-50. The mixture was compacted into an 610 × 500 × 150 mm slab using a LPC-type (Laboratoire des Ponts et Chaussées) roller compactor (NF EN 12697-33 + A1, September 2007). Cylindrical specimens, with a 75 mm diameter and a 150 mm height, were cored and sawn from these slabs. The void content of the specimen R4, whose results are used here, was 3.7%.

3.1.2. Summary description of the tests of the data used

Sinusoidal cyclic DTC tests in strain control mode developed at the University of Lyon / ENTPE were performed on cylindrical specimens. Three types of tests were executed in this thesis: complex modulus test, fatigue test and Advanced Laboratory Fatigue And Biasing Effects Test (ALFABET). For this scientific paper, only the Complex Modulus Tests (CMT) have an interest. They were performed by

applying a sinusoidal loading in axial strain control mode, centred on zero, with a 50 µm/m amplitude and measured with three extensometers placed at 120° from each other and at mid-height of the specimen. Seven temperatures (from −25°C to 40°C) and seven frequencies (from 0.01 Hz to 10 Hz) were applied. In order to obtain the viscoelastic properties on a larger range, two smaller frequencies (0.001 and 0.003 Hz) were added at 40°C. To control temperature, tests were performed inside a thermal chamber. A conditioning time of 4 h was maintained at every temperature change to assure a homogeneous temperature state inside specimens. And a rest period of 300 s was maintained between two consecutive frequencies. In the thesis, the complete experimental data of the specimen R4 from the sample A.0.35-50 are given. Data were retrieved from the thesis by graphical reading with the software 'GetData Graph Digitizer'.

3.2. Getting the experimental curves $\Re_E(\omega)$ and $\Im_\eta(\omega)$

The first step to build the VENoL model consists to identify the experimental stiffness and viscosity components $\Re_E$ and $\Im_\eta$ for the specimen A.0.35-50.R4. They are calculated from the experimental real and imaginary parts $\Re(E^*)$ and $\Im(E^*)$ given by the CMT by using Equation (5). By plotting in a graph the values of $\Re_E$ and $\Im_\eta$ according to the pulsation ω (Figure 2), it seems possible to superpose each isotherm as usual for the norm of the complex stiffness modulus $|E^*|$ and the phase angle φ_{E^*}.

3.3. Application of the Time-Temperature Superposition Principle

For the VENoL model, the Time-Temperature Superposition Principle (TTSP) is characterised by calculating the reduced pulsation ω_{R-T} and the reduced viscosity component $\Im_{\eta,R-T}$ from the application of a translation factor a_T on ω and $\Im_\eta$ (Equations (7) and (8)). If a_T intervenes on $\Im_\eta$, it is because in Equation (5), $\Im_\eta$ is multiplied by ω. And since ω is multiplied by a_T at the TTSP, we must divide $\Im_\eta$ by a_T to keep the equation in balance.

$$\omega_{R-T} = a_T \cdot \omega \tag{7}$$

$$\Im_{\eta,R-T} = \frac{\Im_\eta}{a_T} \tag{8}$$

The factor a_T is calculated with the WLF equation according to the temperature T (Equation (9)). T_{ref} is the chosen reference temperature, $C_{1,aT}$ and $C_{2,aT}$ are two constants. The factor a_T is equal to 1.0 at T_{ref}.

$$\log a_T(T) = \frac{-C_{1,aT} \cdot (T - T_{ref})}{C_{2,aT} + (T - T_{ref})} \tag{9}$$

The TTSP is applied to the specimen A.0.35-50.R4. In his thesis, Mangiafico defined T_{ref} on 14.2°C and calibrated $C_{1,aT}$ and $C_{2,aT}$ respectively on 30.86 and 196.084°C. In this way, two unique experimental curves $\Re_E(\omega_{R-T})$ and $\Im_{\eta,R-T}(\omega_{R-T})$ are obtained (Figure 2). They represent the master curves for $T_{ref} = 14,2^\circ$C.

3.4. Analytical modelling of $\Re_E(\omega_{R-T})$ and $\Im_{\eta,R-T}(\omega_{R-T})$

The last step consists to fit the previous experimental master curves $\Re_E(\omega_{R-T})$ and $\Im_{\eta,R-T}(\omega_{R-T})$. This action will allow us to predict the variations of the components $\Re_E$ and $\Im_\eta$ of the VENoL model according to temperatures and frequencies.

3.4.1. Reduced transition pulsation

The experimental curves $\Re_E(\omega_{R-T})$ and $\Im_{\eta,R-T}(\omega_{R-T})$ show an inflexion point whose position is given by the reduced pulsation of the peak of the phase angle (Figure 3). We called it the transition reduced

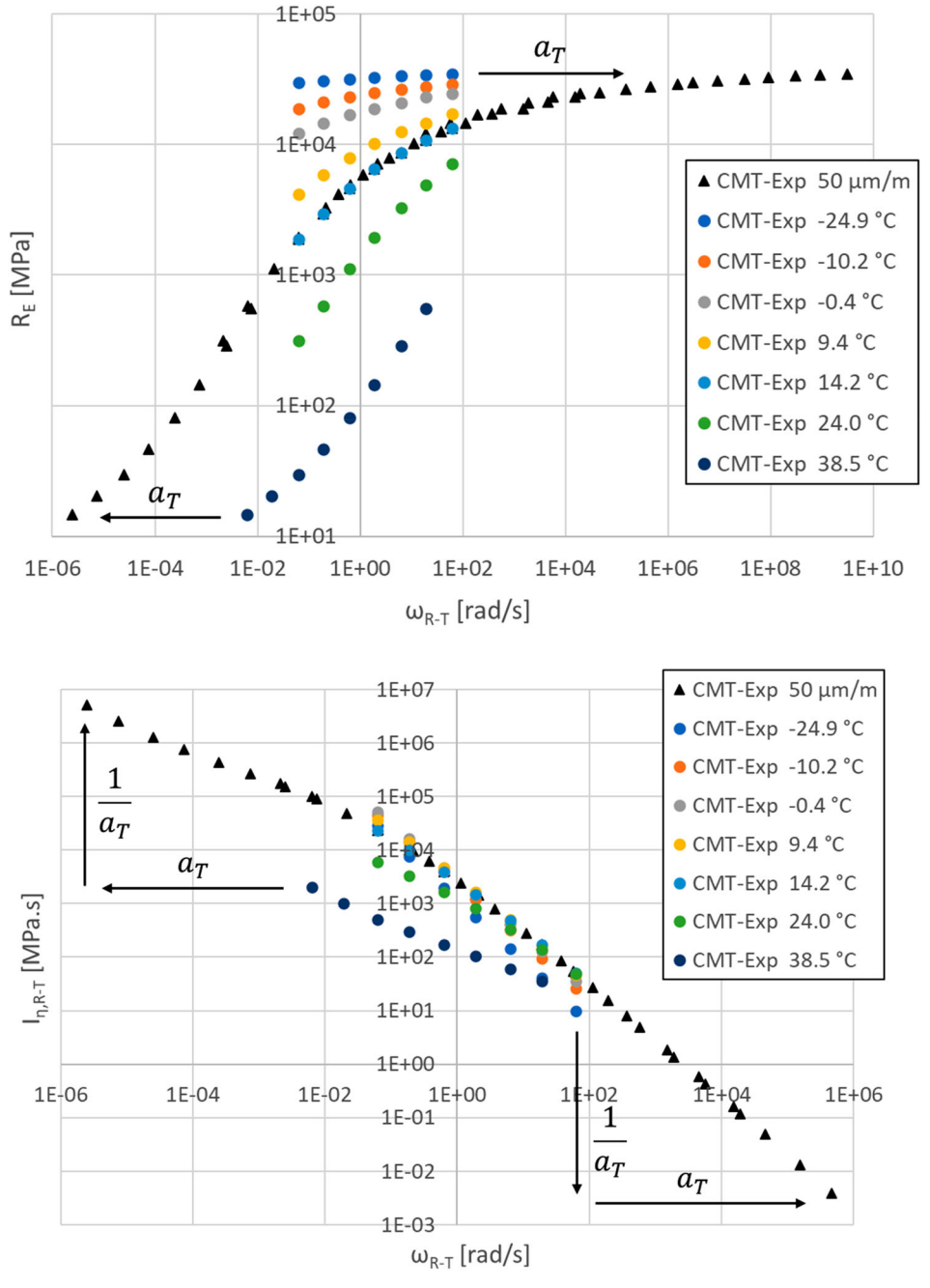

Figure 2. Mangiafico's asphalt concrete – Specimen A.0.35-50.R4 (CMT, 50 µm/m). Plotting of experimental data and application of the TTSP for the stiffness component $\Re_E$ (top) and the reduced viscosity component $\Im_{\eta,R-T}$ (bottom) as a function of the reduced pulsation ω_{R-T}.

pulsation $\omega_{R-T,tr}$. A change in the performances of the material seems to take place around this point surely coming from the influence of aggregates but also from the bitumen structure. Indeed, it is now recognised that the glass transition temperature T_g of bitumen is around −20°C (varies with formulation) and is associated with the maltenes matrix (Lesueur, 2009). But for other authors, there may be

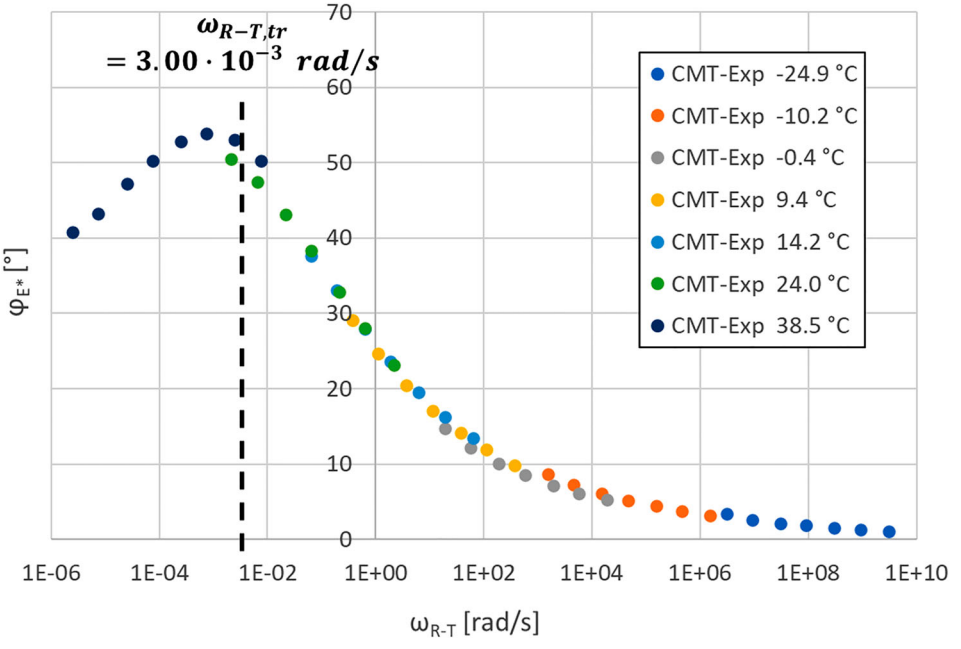

Figure 3. Mangiafico's asphalt concrete – Specimen A.0.35-50.R4 (CMT, 50 µm/m). Plotting of experimental data in the graph 'phase angle φ_{E^*} as a function of the reduced pulsation ω_{R-T}' with the position of the transition reduced pulsation $\omega_{R-T,tr}$.

a second glass transition temperature around 50–70°C associated with asphaltene aggregates (Masson & Polomark, 2001; Mouazen, 2011). In addition, according to Didier Lesueur, TTSP is less effective at high temperatures for bitumen. Mouhamad Mouazen suggested that a second TTSP should be applied to correct this because of the interaction of asphaltenes. Thus, it seems that above $\omega_{R-T,tr}$, the effect of the maltene matrix might predominate in the asphalt concrete behaviour while below $\omega_{R-T,tr}$, the effect of asphaltenes might predominate.

Attempts to calibrate $\Re_E(\omega_{R-T})$ and $\Im_{\eta,R-T}(\omega_{R-T})$ from sigmoid mathematical equations have proved unsuccessful. Therefore, it seems difficult to find a mathematical equation that can fit the entirety of $\Re_E(\omega_{R-T})$ and $\Im_{\eta,R-T}(\omega_{R-T})$. The most practical solution is to separate each of the curves in two at the level of $\omega_{R-T,tr}$ and to model them separately. Each part may be modelled with a Carreau–Yasuda model equation. For the needs of the modelling to come, $\omega_{R-T,tr}$ is defined at $3.00 \cdot 10^{-3}$rad/s.

3.4.2. Carreau–Yasuda model

Carreau–Yasuda (CY) model describes the apparent viscosity of a non-Newtonian fluid as a function of the shear rate $\dot{\gamma}$. It consists of five parameters (Equation (10) and example Figure 4, blue curve). In frequency analysis, the shear rate is replaced by the pulsation (or frequency) in Equation (10). The model was first proposed by Pierre Carreau with $a = 2$ in 1958 (Byron Bird & Carreau, 1968). Kenji Yasuda then generalised the model in 1979 with a taking any value (Yasuda, 1979).

At a low shear rate ($\dot{\gamma} \ll 1/\lambda$), a Carreau–Yasuda fluid behaves as a Newtonian fluid with viscosity η_{up}. At intermediate shear rates ($\dot{\gamma} \gtrsim 1/\lambda$), a CY fluid behaves as a power-law fluid which depends on the power index n. At a high shear rate, a CY fluid behaves as a Newtonian fluid again with the viscosity η_{low}.

$$\eta = \eta_{low} + (\eta_{up} - \eta_{low}) \cdot [1 + (\lambda \cdot \dot{\gamma})^a]^{\frac{n-1}{a}} \tag{10}$$

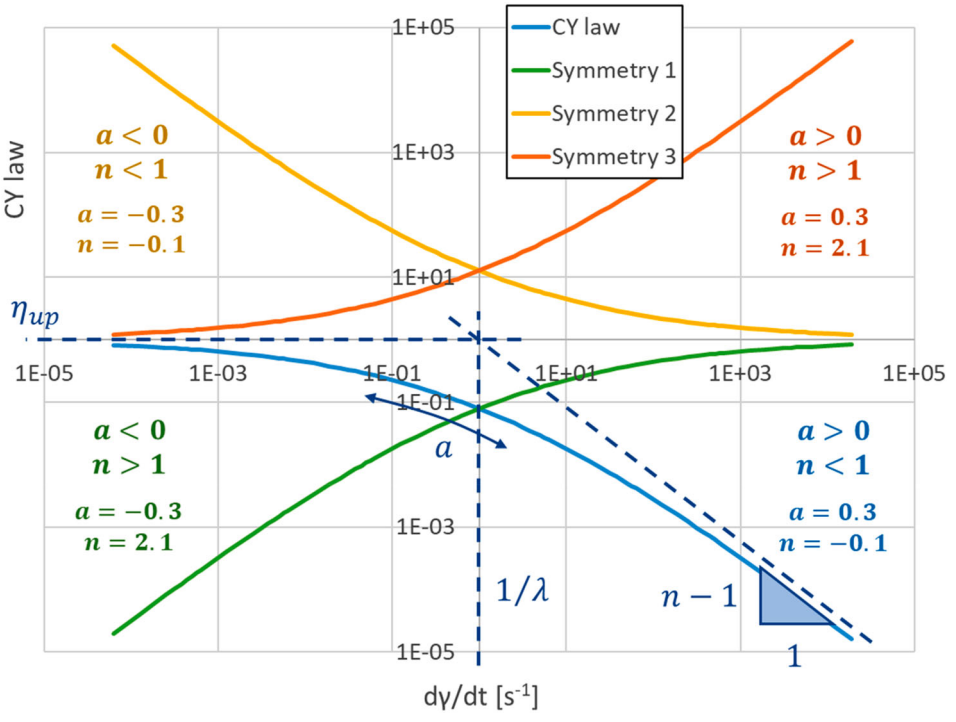

Figure 4. Values of a and n used to construct an example representation of the Carreau-Yasuda model with its symmetries. $\eta_{low} =$ 0Pa.s, $\eta_{up} = 1$Pa.s, $\lambda = 1$s.

where, η_{low} is the lower Newtonian plateau (or viscosity at the infinite shear rate) [Pa.s]; η_{up} is the upper Newtonian plateau (or viscosity at zero shear rate) [Pa.s]; λ is the characteristic time controlling the intersection position of the upper Newtonian plateau and the slope [s]; n is the power index controlling the area in power law ($n < 1$, identical to that of Ostwald model) [-]; a is the power index describing the transition between the upper Newtonian plateau and the slope ($a > 0$) [-].

Besides its main function of describing the viscosity, the CY model is also of great mathematical interest since it draws a sigmoid in a logarithmic coordinates space with control of the slope $n - 1$. However, the lower plateau η_{low} is not of interest for modelling the $\Re_E(\omega_{R-T})$ and $\Im_{\eta,R-T}(\omega_{R-T})$ curves. This makes the model more interesting since it is now possible to obtain its axial symmetries, according to the vertical axis formed by $1/\lambda$ and the horizontal axis formed by η_{up}, by simply modifying the signs of its coefficients a and $n - 1$ (Figure 4). Therefore, it is possible to model with a single type of mathematical equation all the variations of the curves $\Re_E(\omega_{R-T})$ and $\Im_{\eta,R-T}(\omega_{R-T})$.

An additional argument in favour of using the CY model is found in the differential equation of the Maxwell model, composed of a spring of elasticity E and a dashpot of viscosity η connected in series (Equation (11)). In frequency analysis, the Maxwell equation can also be written with the CY model to describe the variations of $\Re_E$ and $\Im_\eta$ components along ω (Equations (12)–(14)). Equation (14) shows that the Maxwell model can be written as a Kelvin–Voigt model with variable parameters. The values of the CY model exponents are defined as such: $a = -2$, $n = 3$ for $\Re_E$ and $a = 2$, $n = -1$ for $\Im_\eta$. We find for a, the value 2 of Pierre Carreau's original model.

However, many materials have behaviours that differ from these fixed values, such as bituminous mixtures. The Generalised Maxwell model, composed of Maxwell elements in parallel, adds Carreau models ($a = 2$) with different combinations of E and η to reproduce the asphalt concrete behaviour. Thus, after a good calibration, an apparent slope and a slope/plateau transition zone are normally obtained whose respective apparent coefficients a and n differ from the fixed values. The VENoL model

overcomes these constraints by directly modifying the parameters of the CY model at the source rather than looking for a combination of rheological models that can reproduce it.

$$\dot{\varepsilon}^*_{MX}(t) = \frac{\sigma^*_{MX}(t)}{\eta} + \frac{\dot{\sigma}^*_{MX}(t)}{E} \tag{11}$$

$$\begin{cases} \dot{\sigma}^*_{MX}(t) = i\omega \cdot \sigma^*_{MX}(t) \\ \dot{\varepsilon}^*_{MX}(t) = i\omega \cdot \varepsilon^*_{MX}(t) \end{cases} \tag{12}$$

$$\sigma^*_{MX}(t) = \boldsymbol{E} \cdot [1 + (\boldsymbol{\lambda\omega})^{-2}]^{-1} \cdot \varepsilon^*_{MX}(t) + \boldsymbol{\eta} \cdot [1 + (\boldsymbol{\lambda\omega})^{2}]^{-1} \cdot \dot{\varepsilon}^*_{MX}(t) \tag{13}$$

With, $\lambda = \frac{\eta}{E}$

$$\sigma^*_{MX}(t) = \Re_{\boldsymbol{E}}(\boldsymbol{\omega}) \cdot \varepsilon^*_{MX}(t) + \Im_{\boldsymbol{\eta}}(\boldsymbol{\omega}) \cdot \dot{\varepsilon}^*_{MX}(t) \tag{14}$$

3.4.3. Modelling

By composing with the CY model and its symmetries, the variations of the stiffness component $\Re_E$ (green curves on Figure 5) and the reduced viscosity component $\Im_{\eta,R-T}$ (red curves) can be defined as a function of the reduced pulsation ω_{R-T}, below (dotted curves) and above (continuous curves) the transition reduced pulsation $\omega_{R-T,tr}$. CY parameters names are changed to correspond with the VENoL model (Equations (15) and (16)): $\Re_{E,low,1}$, $\Im_{\eta,R-T,low,1}$ and $\Re_{E,up,2}$, $\Im_{\eta,R-T,up,2}$ [MPa, MPa.s] are respectively lower and upper bounds, λ [s/rad] controls the position of the slope/bound intersection on the axis ω_{R-T}, n [-] is the slope coefficient and k [-] is the slope/bound transition coefficient. These

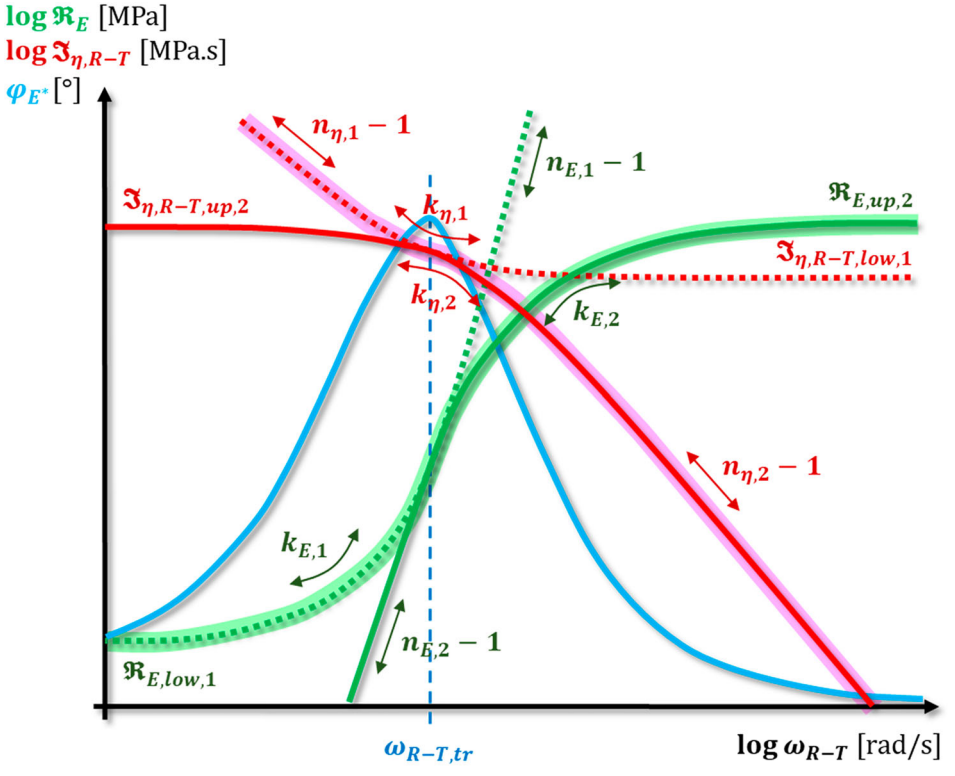

Figure 5. Illustration of variations of the stiffness component $\Re_E$ and the reduced viscosity component $\Im_{\eta,R-T}$ as a function of the reduced pulsation ω_{R-T}. The peak of the phase angle φ_{E^*} gives the transition reduced pulsation $\omega_{R-T,tr}$.

Table 2. Mangiafico's asphalt concrete. Modelling parameters of the CY model for the references master curves $\Re_E(\omega_{R-T})$ and $\Im_{\eta,R-T}(\omega_{R-T})$ at $T_{ref} = 14,2°C$.

Transition reduced pulsation:		$\omega_{R-T,tr} = 3.00 \cdot 10^{-3}$rad/s	
$\Re_E(\omega_{R-T})$		$\Im_{\eta,R-T}(\omega_{R-T})$	
$\omega_{R-T} \leq \omega_{R-T,tr}$	$\omega_{R-T} \geq \omega_{R-T,tr}$	$\omega_{R-T} \leq \omega_{R-T,tr}$	$\omega_{R-T} \geq \omega_{R-T,tr}$
$R_{E,low,1} = 5.0$MPa	$R_{E,up,2} = 36,000$MPa	$I_{\eta,R-T,low,1} = 3.00 \cdot 10^4$MPa.s	$I_{\eta,R-T,up,2} = 2.40 \cdot 10^6$MPa.s
$\lambda_{E,R-T,1} = 7.00 \cdot 10^0$s/rad	$\lambda_{E,R-T,2} = 1.80 \cdot 10^4$s/rad	$\lambda_{\eta,R-T,1} = 1.00 \cdot 10^4$s/rad	$\lambda_{\eta,R-T,2} = 1.80 \cdot 10^2$s/rad
$k_{E,1} = 0.210$	$k_{E,2} = -0.170$	$k_{\eta,1} = -0.220$	$k_{\eta,2} = 0.250$
$n_{E,1} = 3.460$	$n_{E,2} = 2.900$	$n_{\eta,1} = 0.040$	$n_{\eta,2} = -0.110$

parameters must be calibrated for the reference curve with the condition T_{ref}.

$$\Re_E(T,\omega) = \begin{cases} \text{if } \omega_{R-T} \leq \omega_{R-T,tr}, \\ \Re_{E,low,1} \cdot [1 + [\lambda_{E,R-T,1} \cdot \omega_{R-T}]^{k_{E,1}}]^{\frac{n_{E,1}-1}{k_{E,1}}} \\ ---------- \\ \text{if } \omega_{R-T} \geq \omega_{R-T,tr}, \\ \Re_{E,up,2} \cdot [1 + [\lambda_{E,R-T,2} \cdot \omega_{R-T}]^{k_{E,2}}]^{\frac{n_{E,2}-1}{k_{E,2}}} \end{cases} \tag{15}$$

$k_{E,1} > 0; n_{E,1} > 1; k_{E,2} < 0; n_{E,2} > 1$

$$\Im_{\eta,R-T}(T,\omega) = \begin{cases} \text{if } \omega_{R-T} \leq \omega_{R-T,tr}, \\ \Im_{\eta,R-T,low,1} \cdot [1 + [\lambda_{\eta,R-T,1} \cdot \omega_{R-T}]^{k_{\eta,1}}]^{\frac{n_{\eta,1}-1}{k_{\eta,1}}} \\ ---------- \\ \text{if } \omega_{R-T} \geq \omega_{R-T,tr}, \\ \Im_{\eta,R-T,up,2} \cdot [1 + [\lambda_{\eta,R-T,2} \cdot \omega_{R-T}]^{k_{\eta,2}}]^{\frac{n_{\eta,2}-1}{k_{\eta,2}}} \end{cases} \tag{16}$$

$k_{\eta,1} < 0; n_{\eta,1} < 1; k_{\eta,2} > 0; n_{\eta,2} < 1$

The modelling parameters used for the specimen A.0.35-50.R4 are given in Table 2. The fit of the components $\Re_E$ and $\Im_{\eta,R-T}$ seems correct (Figure 6). The identification of the parameter $1/\lambda$ from experimental data is not always obvious. Indeed, the transition from one equation to another at $\omega_{R-T,tr}$ occurs even before the slope / bound rounded transition is complete. Therefore, the slope does not yet appear. It is then necessary to test several values to find the right one.

To be certain of the modelling, it is necessary to check it in the Cole–Cole and Black spaces which are very sensitive to the variation of parameters (Figure 7). The fit is also correct in these spaces here. Thus, the use of the CY model and its symmetries is justified.

4. Building the VENoL model: adding the influence of strain amplitude

4.1. Use of Graziani's experimental data

As we already mentioned in the introduction, in a part of their scientific paper published in 2019, Graziani et al. carried out some DTC tests on asphalt concrete at three different levels of small strain amplitudes (Graziani et al., 2019). To implement the strain amplitude effects in the VENoL model, these experimental data are reused.

4.1.1. Summary description of the specimen analysed

For the experimentation, the authors considered an asphalt concrete for wearing course produced in a central asphalt plant. The bitumen binder of penetration grade 70/100 was dosed at 5.3% by the

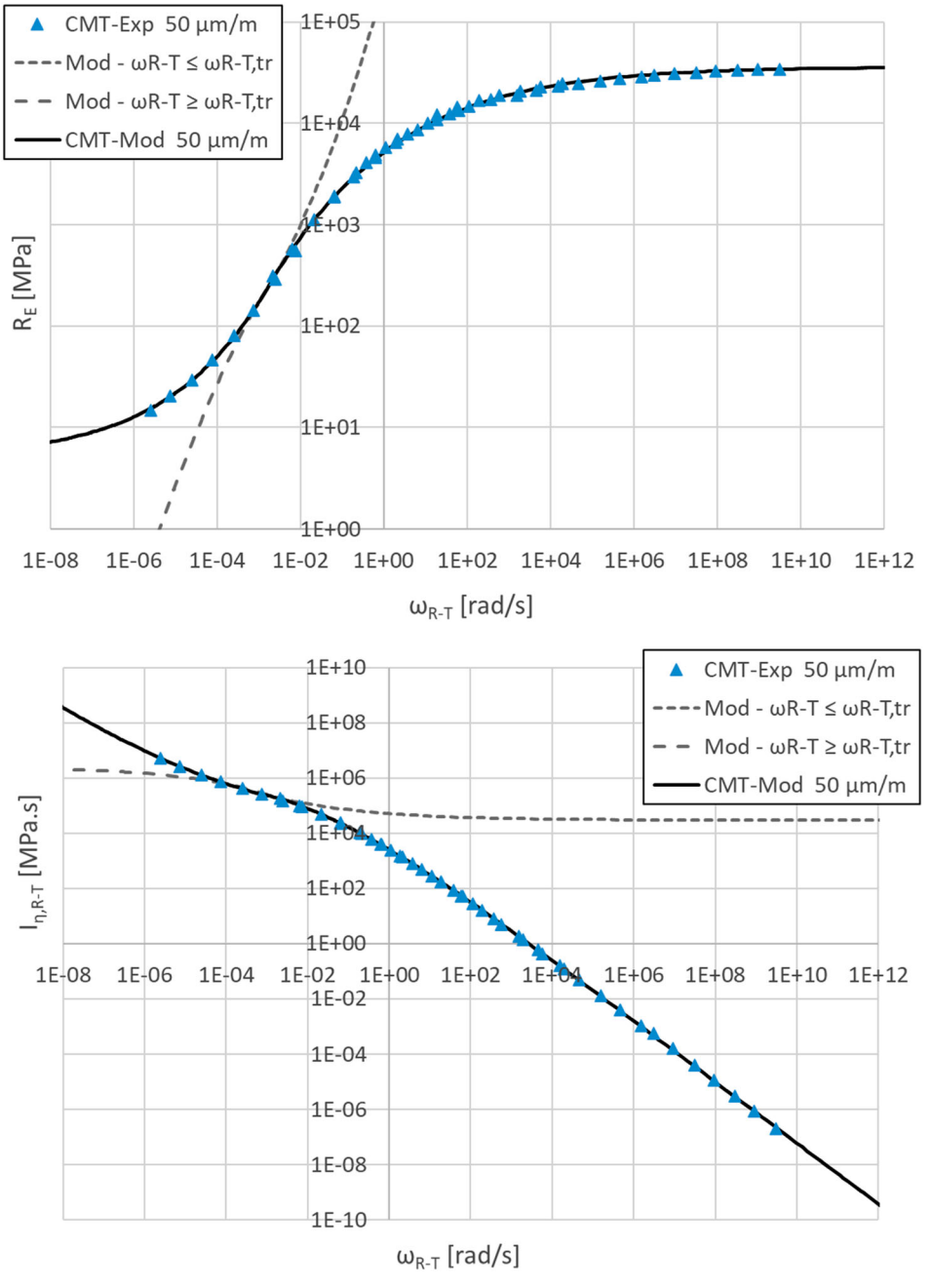

Figure 6. Mangiafico's asphalt concrete – Specimen A.0.35-50.R4 (CMT, 50 µm/m). Plotting of experimental data and fit with the VENoL(T,ω) model for the stiffness component $\Re_E$ (top) and the reduced viscosity component $\Im_{\eta,R-T}$ (bottom) as a function of the reduced pulsation ω_{R-T}. The unused parts of the CY models are plotted in dotted lines.

weight of the final mix. The mixture was characterised by a dense-grading curve with a nominal maximum aggregate size of 11 mm. Cylindrical specimens were produced using a gyratory compactor to a diameter of 150 mm, before being cored to a diameter of 94 mm and cut to a length of 120 mm. The void content for the specimens S1 and S2, whose results are used in this paper, were respectively 9.6% and 8.5%.

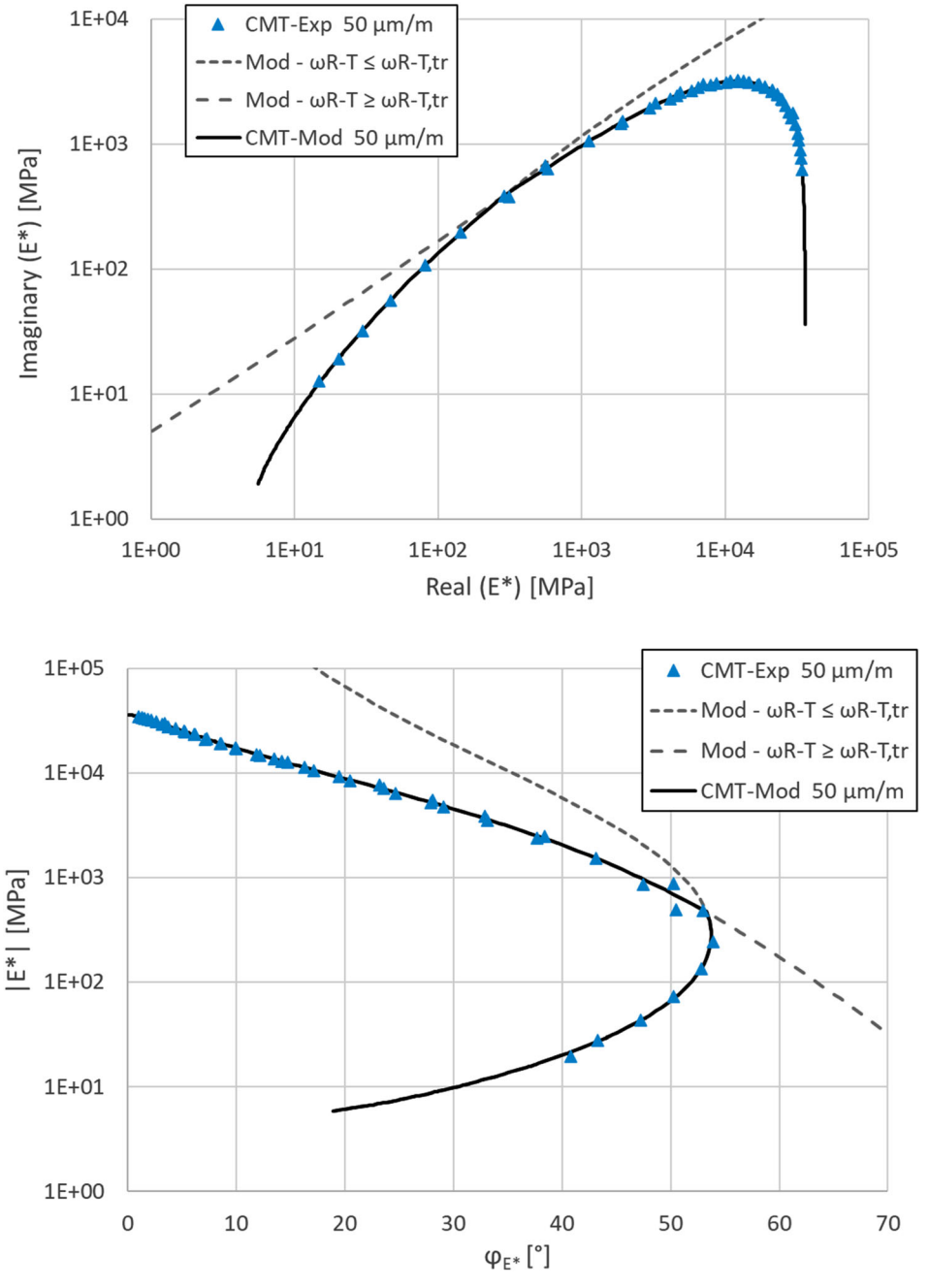

Figure 7. Mangiafico's asphalt concrete – Specimen A.0.35-50.R4 (CMT, 50 µm/m). Plotting of experimental data and fit with the VENoL(T,ω) model in the Cole-Cole (top) and Black (bottom) spaces. The unused parts of CY models are plotted in dotted lines. The Cole-Cole space is represented with logarithmic coordinates to see the dotted lines.

4.1.2. Summary description of the tests of the data used

Sinusoidal cyclic DTC tests were applied on the specimens using a servo-hydraulic press developed at the transportation infrastructure laboratory of the Università Politecnica delle Marche. The tests were carried out in a control stress mode and the applied stress amplitude was adjusted to obtain the desired steady state strain amplitude, measured with two axial strain gauges at mid-height of the

specimen. To evaluate nonlinearity, three levels of strain amplitude (15, 30 and 60 μm/m), centred on zero, were performed with frequency sweeps at five temperatures (0, 10, 20, 30 and 40°C) and five frequencies (0.1, 0.25, 1, 4 and 12 Hz). Therefore, that is a total of seventy-five cyclic tests. Each test consisted in applying twenty loading cycles, starting from the lower strain level, the lower temperature, and the higher frequency. A thermal chamber was used to control the temperature during the tests. A rest period of at least ten minutes was maintained between two consecutive frequencies. The measured stress and strain signals were used to evaluate the complex moduli. Data obtained for each test of the specimens S1 and S2 were provided to us by the authors of the paper.

4.2. Application of the VENoL model for the reference strain amplitude

Before studying nonlinearity, the experimental data are separated into two groups. The medium strain amplitude of 30 μm/m is considered as the reference $\varepsilon_{0,ref}$. It belongs to the group Complex Modulus Test (CMT). And the strain amplitudes 15 and 60 μm/m belong to the NonLinearity Tests (NLT).

The method developed in part 3 to build the VENoL(T,ω) model is applied to the CMT. The reference temperature T_{ref} is taken equal to 20°C. The TTSP is applied with the WLF equation. The coefficients $C_{1,aT}$ and $C_{2,aT}$ are respectively defined equal to 13.6 and 92.8°C for the two specimens S1 and S2. These WLF parameters were defined by Graziani et al. in their scientific paper. They are the same parameters for the three different strain amplitudes because the TTSP applies within the NLVE region (see section 1.1). The experimental master curves of $\Re_E$ and $\Im_{\eta,R-T}$ for $T_{ref} = 20°C$ and $\varepsilon_{0,ref} = 30\mu m/m$ become the frame of reference. They are fitted with the CY model (Equations (15) and (16)). The modelling parameters used for the specimens S1 and S2 are given in Table 3. The transition reduced pulsation $\omega_{R-T,tr}$ is fixed at $3.00 \cdot 10^{-2}$rad/s for the specimen S1 and at $6.00 \cdot 10^{-3}$rad/s for the specimen S2. Below $\omega_{R-T,tr}$, there are not enough experimental points; the fits are therefore partially assumed. The fits of the components $\Re_E$ and $\Im_{\eta,R-T}$ seems correct, as we can check it in the Cole–Cole space (Figure 8). Using different experimental data confirms the method developed in part 3.

In this Figure 8, the experimental data for the two specimens are quite different although they have the same composition. The two experimental curves have a similar shape and only seem to differ by one scale factor. This difference may be explained by their void content; the specimen S1 is less dense than the specimen S2. During the analytical modelling process, the fit was first performed on the specimen S2. The experimental data for the specimen S1 was then calibrated using the same parameters k_E, n_E and k_η, n_η, but varying the parameters $\omega_{R-T,tr}$, $\lambda_{E,R-T}$, $\lambda_{\eta,R-T}$ and $R_{E,low}$, $R_{E,up}$, $I_{\eta,R-T,low}$, $I_{\eta,R-T,up}$. As k_E, n_E and k_η, n_η are shape coefficients, it would appear that the shape of the curve is uniquely related to the viscoelastic behaviour of the bituminous binder. The parameters $\omega_{R-T,tr}$, $\lambda_{E,R-T}$ and $\lambda_{\eta,R-T}$ influence the position of the curves of the stiffness and reduced viscosity components $\Re_E$ and $\Im_{\eta,R-T}$ according to the reduced pulsation. And the parameters $R_{E,low}$, $R_{E,up}$ and $I_{\eta,R-T,low}$, $I_{\eta,R-T,up}$ on

Table 3. Graziani's asphalt concrete – Specimens S1 and S2. Modelling parameters of the CY model for the reference master curves $\Re_E(\omega_{R-T})$ and $\Im_{\eta,R-T}(\omega_{R-T})$ at $T_{ref} = 20°C$ and $\varepsilon_{0,ref} = 30\mu m/m$.

	$\Re_E(\omega_{R-T})$		$\Im_{\eta,R-T}(\omega_{R-T})$	
S1	Transition reduced pulsation:		$\omega_{R-T,tr} = 3.00 \cdot 10^{-2}$rad/s	
	$\omega_{R-T} \leq \omega_{R-T,tr}$	$\omega_{R-T} \geq \omega_{R-T,tr}$	$\omega_{R-T} \leq \omega_{R-T,tr}$	$\omega_{R-T} \geq \omega_{R-T,tr}$
	$R_{E,low,1} = 80.0$MPa	$R_{E,up,2} = 23,100$MPa	$I_{\eta,R-T,low,1} = 1.80 \cdot 10^3$MPa.s	$I_{\eta,R-T,up,2} = 5.80 \cdot 10^5$MPa.s
	$\lambda_{E,R-T,1} = 3.90 \cdot 10^1$s/rad	$\lambda_{E,R-T,2} = 1.20 \cdot 10^3$s/rad	$\lambda_{\eta,R-T,1} = 1.30 \cdot 10^0$s/rad	$\lambda_{\eta,R-T,2} = 8.30 \cdot 10^1$s/rad
S2	Transition reduced pulsation:		$\omega_{R-T,tr} = 6.00 \cdot 10^{-3}$rad/s	
	$\omega_{R-T} \leq \omega_{R-T,tr}$	$\omega_{R-T} \geq \omega_{R-T,tr}$	$\omega_{R-T} \leq \omega_{R-T,tr}$	$\omega_{R-T} \geq \omega_{R-T,tr}$
	$R_{E,low,1} = 80.0$MPa	$R_{E,up,2} = 26,500$MPa	$I_{\eta,R-T,low,1} = 1.29 \cdot 10^4$MPa.s	$I_{\eta,R-T,up,2} = 2.63 \cdot 10^6$MPa.s
	$\lambda_{E,R-T,1} = 2.00 \cdot 10^2$s/rad	$\lambda_{E,R-T,2} = 4.40 \cdot 10^3$s/rad	$\lambda_{\eta,R-T,1} = 1.10 \cdot 10^1$s/rad	$\lambda_{\eta,R-T,2} = 3.30 \cdot 10^2$s/rad
Both	$k_{E,1} = 0.300$	$k_{E,2} = -0.166$	$k_{\eta,1} = -0.550$	$k_{\eta,2} = 0.260$
	$n_{E,1} = 1.946$	$n_{E,2} = 2.290$	$n_{\eta,1} = 0.330$	$n_{\eta,2} = -0.085$

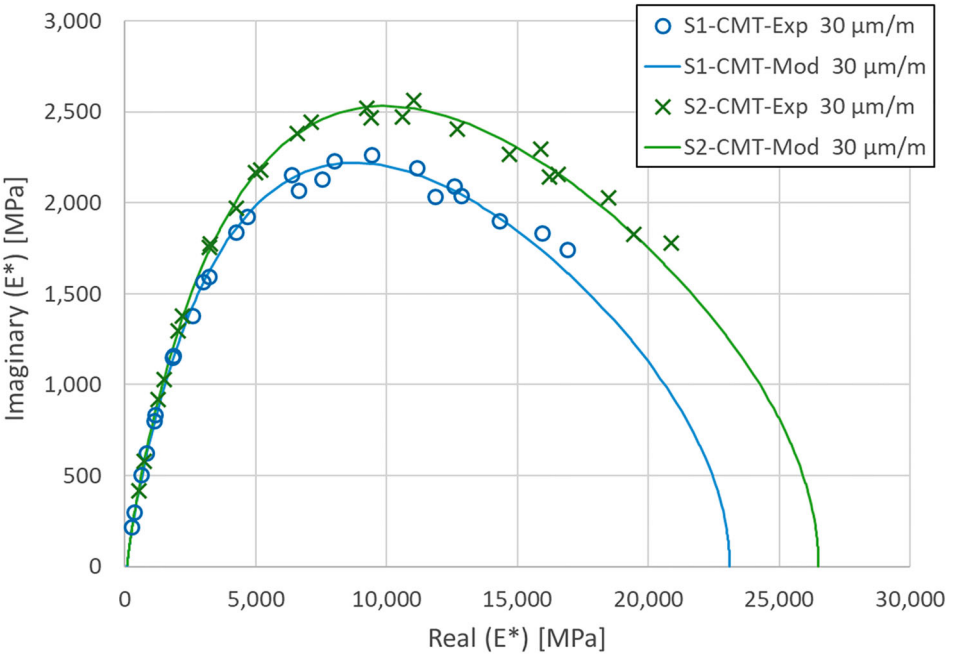

Figure 8. Graziani's asphalt concrete – Specimens S1 and S2 (CMT). Plotting of experimental data in the Cole-Cole space and fit with the VENoL(T,ω) model.

their bounds. Thus, the granular skeleton seems to impact the position of the curves of $\Re_E$ and $\Im_{\eta,R-T}$ according to the reduced pulsation as well as on their scale.

4.3. Observation of the nonlinearity effect on experimental data

The experimental points of the NLTs and the referential CMT are quite distinct in the graphic $\Re_E(\omega_{R-T})$ facilitating observations (Figure 9, top). Thus, it appears that the variations of $\Re_E$ for each strain amplitude levels seem to follow identical shapes but shifted depending on the ω_{R-T} axis. They seem to tend towards the same limit value of $\Re_E$ at high reduced pulsation. Therefore, it could be interesting to set up a translation factor a_A ('A' for amplitude) based on the same principle as the coefficient a_T of the TTSP.

However, due to the rapid evolution of $\Im_{\eta,R-T}$ (power law), it is difficult to make a further observation since the data for each amplitude are too tight in the logarithmic plot (Figure 9, bottom). We need to look at another graph.

The observation of experimental data in the Cole–Cole space allows us to understand that the establishment of a_A is not sufficient to describe the nonlinearity effect (Figure 10). Indeed, the coefficient a_T, whose a_A is based on the same structure, only allows the points to be slid along the modelled curve of the CMT. However, nonlinearity also influences the height of the curve, it means only the imaginary part. To apply this effect, it is necessary to create a second translation factor, named b_A, acting only on $\Im_{\eta,R-T}$.

4.4. Creating a new superposition principle

4.4.1. Time-Amplitude Semi-Superposition Principle

The two translation factors a_A and b_A defined previously form the Time-Amplitude Semi-Superposition Principle (TASSP). It connects strain amplitude and pulsation. As for the factor a_T with the TTSP, the

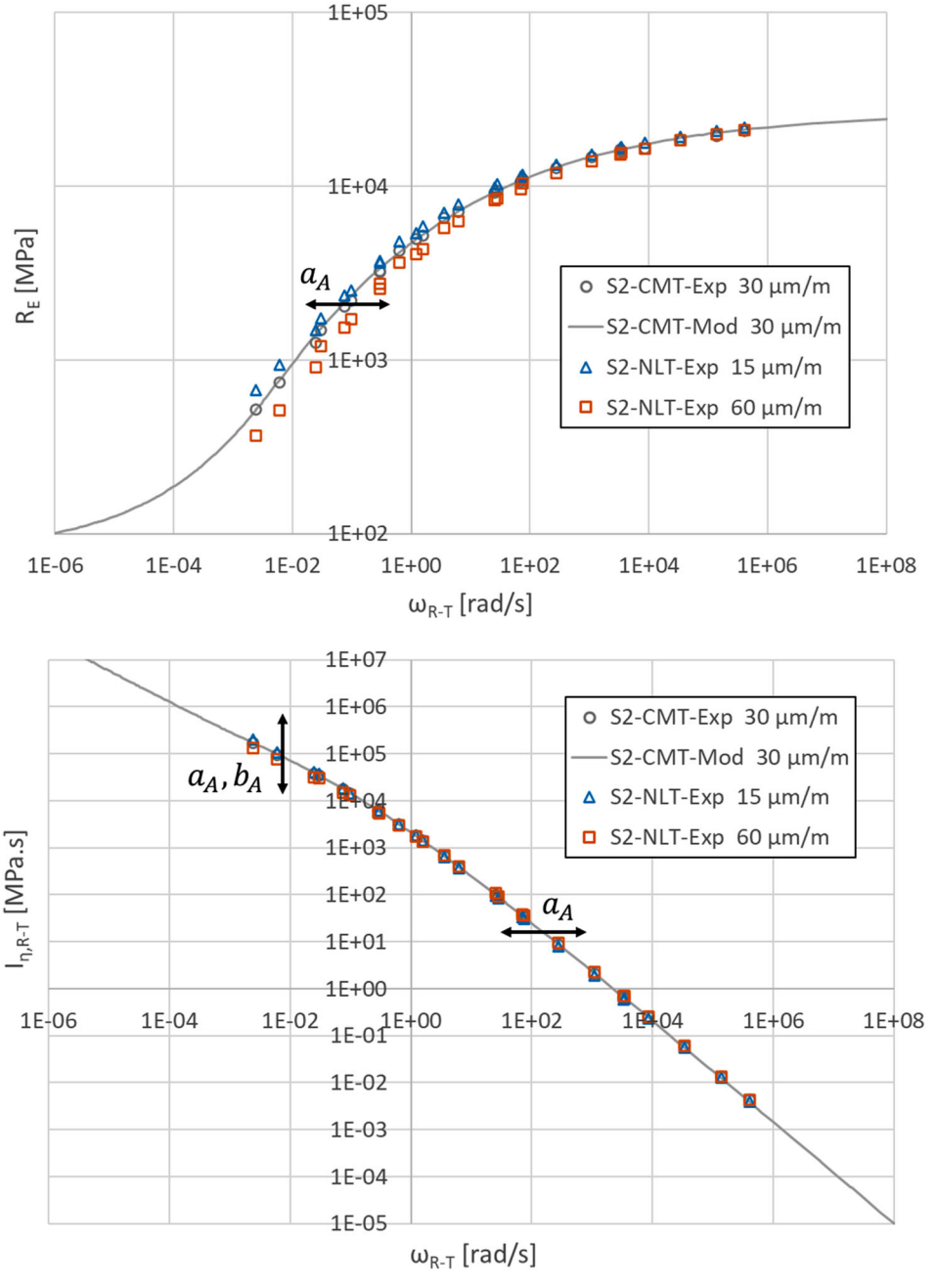

Figure 9. Graziani's asphalt concrete – Specimen S2 (CMT, 30 µm/m and NLTs, 15/60 µm/m). Plotting of experimental data and comparison between CMT and NLTs for the stiffness component $\Re_E$ (top) and the reduced viscosity component $\Im_{\eta,R-T}$ (bottom) according to the reduced pulsation ω_{R-T}. Fitting of the CMT at $\varepsilon_{0,ref} = 30\mu m/m$ with the VENoL(T,ω) model.

factor a_A intervenes on the reduced pulsation ω_{R-A} and on the reduced viscosity component $\Im_{\eta,R-A}$ (Equations (17) and (18)). The factor b_A is a correction coefficient that only affects $\Im_{\eta,R-A}$ (Equation (18)). That is why the term semi-superposition is used. The factors a_A and b_A are equal to 1.0 at $\varepsilon_{0,ref}$.

$$\omega_{R-A} = a_A \cdot \omega \tag{17}$$

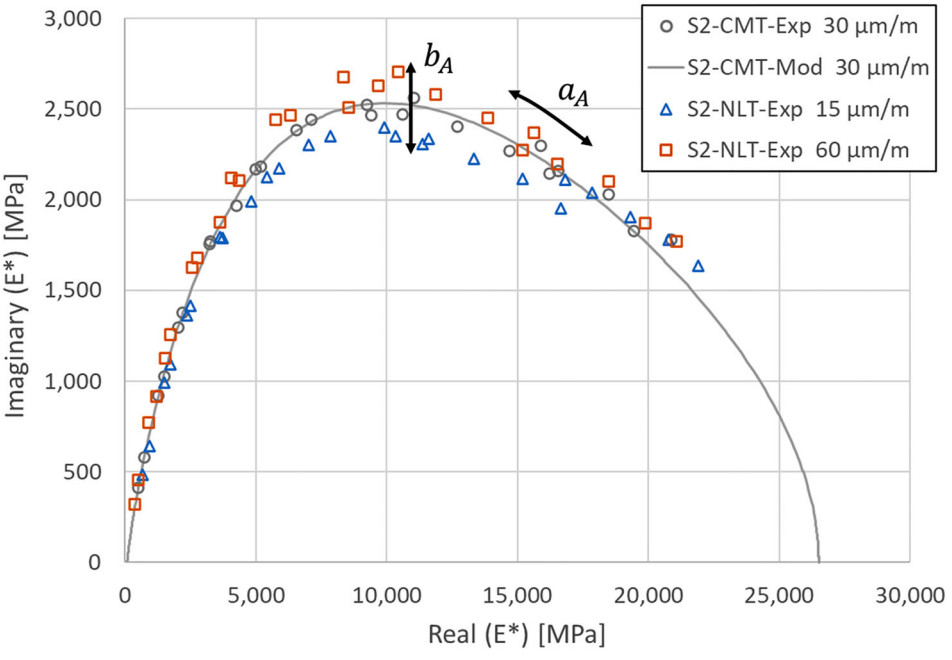

Figure 10. Graziani's asphalt concrete – Specimen S2 (CMT, 30 µm/m and NLTs, 15/60 µm/m). Plotting of experimental data in the Cole-Cole space and comparison between CMT and NLTs. Fitting of the CMT at $\varepsilon_{0,ref} = 30\mu m/m$ with the VENoL(T,ω) model.

$$\Im_{\eta,R-A} = \frac{\Im_\eta}{a_A \cdot b_A} \tag{18}$$

4.4.2. Time-Temperature-Amplitude Semi-Superposition Principle

The combination of the TTSP and the TASSP gives the Time-Temperature-Amplitude Semi-Superposition Principle (TTASSP). It is characterised by the translation factors a_{TA} (Equation (19)) and b_A. For the reference conditions, a_{TA} and b_A are equal to 1.0. The combination allows us to calculate the reduced pulsation ω_{R-TA} (Equation (20)) and the reduced viscosity component $\Im_{\eta,R-TA}$ (Equation (21)).

$$a_{TA} = a_T \cdot a_A \tag{19}$$

$$\omega_{R-TA} = a_{TA} \cdot \omega \tag{20}$$

$$\Im_{\eta,R-TA} = \frac{\Im_\eta}{a_{TA} \cdot b_A} \tag{21}$$

4.4.3. Evolution of Equations (15) ($\Re_E$) and (16) ($\Im_{\eta,R-T}$)

The CMT at 20°C and 30 µm/m of each specimen is the frame of reference for the TTASSP. The parameters names resulting from the CY model (Equations (15) and (16)) defining the stiffness and viscosity components $\Re_E$ and $\Im_\eta$ evolve but their values remain the same since a_{TA} and b_A are equal to 1.0 for the referential conditions (Table 4).

4.5. Identification of TASSP factors laws

4.5.1. Calculation of the values of $a_{A,exp}(\varepsilon_0)$ and $b_{A,exp}(\varepsilon_0)$

By applying a couple of shift factors a_A and b_A to the CMT modelling, it is possible to find the results of a NLT modelling at the desired amplitude. However, the variation laws $a_A(\varepsilon_0)$ and $b_A(\varepsilon_0)$ must be

Table 4. VENoL(T,ω,ϵ_0) model. Evolution of the parameters naming of the CY model defining the stiffness and viscosity components $\Re_E$ and $\Im_\eta$ according to the principle used.

Parameters	TTSP	TTASSP
Transition reduced pulsation [rad/s]	$\omega_{R-T,tr}$	$\omega_{R-TA,tr}$
Stiffness component – Parameter 1 controlling the position of the curve on the axis ω [s/rad]	$\lambda_{E,R-T,1}$	$\lambda_{E,R-TA,1}$
Stiffness component – Parameter 2 controlling the position of the curve on the axis ω [s/rad]	$\lambda_{E,R-T,2}$	$\lambda_{E,R-TA,2}$
Viscosity component – Lower bound [MPa.s]	$\Im_{\eta,R-T,low,1}$	$\Im_{\eta,R-TA,low,1}$
Viscosity component – Parameter 1 controlling the position of the curve on the axis ω [s/rad]	$\lambda_{\eta,R-T,1}$	$\lambda_{\eta,R-TA,1}$
Viscosity component – Upper bound [MPa.s]	$\Im_{\eta,R-T,up,2}$	$\Im_{\eta,R-TA,up,2}$
Viscosity component – Parameter 2 controlling the position of the curve on the axis ω [s/rad]	$\lambda_{\eta,R-T,2}$	$\lambda_{\eta,R-TA,2}$

identified. For each strain amplitude and each experimental point (T, ω), it is therefore necessary to calculate a pair of experimental factors $a_{A,exp}$ and $b_{A,exp}$. They are isolated from Equations (15) and (16) to which Table 4 has been applied. Then, the factors are estimated by applying Equation (22) followed by (23).

$$a_{A,exp} = \begin{cases} if\ \Re_{E,exp} \le \Re_E(\omega_{R-TA,tr}), \\ \frac{1}{\lambda_{E,R-TA,1}\cdot\omega_{R-T,exp}} \cdot \left[\left[\frac{\Re_{E,exp}}{\Re_{E,low,1}}\right]^{\frac{k_{E,1}}{n_{E,1}-1}} - 1\right]^{\frac{1}{k_{E,1}}} \\ - \\ if\ \Re_{E,exp} \ge \Re_E(\omega_{R-TA,tr}), \\ \frac{1}{\lambda_{E,R-TA,2}\cdot\omega_{R-T,exp}} \cdot \left[\left[\frac{\Re_{E,exp}}{\Re_{E,up,2}}\right]^{\frac{k_{E,2}}{n_{E,2}-1}} - 1\right]^{\frac{1}{k_{E,2}}} \end{cases} \quad (22)$$

$$b_{A,exp} = \begin{cases} if\ a_{A,exp}\cdot\omega_{R-T,exp} \le \omega_{R-TA,tr}, \\ \frac{\Im_{\eta,R-T,exp}}{\Im_{\eta,R-TA,low,1}\cdot a_{A,exp}} \cdot [1 + [\lambda_{\eta,R-TA,1}\cdot a_{A,exp}\cdot\omega_{R-T,exp}]^{k_{\eta,1}}]^{-\frac{n_{\eta,1}-1}{k_{\eta,1}}} \\ - \\ if\ a_{A,exp}\cdot\omega_{R-T,exp} \ge \omega_{R-TA,tr}, \\ \frac{\Im_{\eta,R-T,exp}}{\Im_{\eta,R-TA,up,2}\cdot a_{A,exp}} \cdot [1 + [\lambda_{\eta,R-TA,2}\cdot a_{A,exp}\cdot\omega_{R-T,exp}]^{k_{\eta,2}}]^{-\frac{n_{\eta,2}-1}{k_{\eta,2}}} \end{cases} \quad (23)$$

For specimen S2, the dispersion of experimental factors $a_{A,exp}$ and $b_{A,exp}$ according to ω_{R-T} does not seem to follow any particular trend (Figure 11). The same observation has been obtained for specimen S1. Thus, the factors seem to be independent of temperature and frequency for small strains. For each factor and strain amplitude, a constant is therefore defined by taking the median (value displayed on the graphs). The median is chosen because, unlike the average, it is much less influenced by extreme results. But the average was also calculated, and the values obtained were almost equal to the median. This methodology was also applied to the experimental data at 30 µm/m to verify the good fit of the CMT modelling; $a_{A,exp}$ and $b_{A,exp}$ must be close to 1.00 for this amplitude. The results are correct.

4.5.2. Verification of the superposition effect on the norm of the complex stiffness modulus with $a_{A,exp}(\varepsilon_0)$ and $b_{A,exp}(\varepsilon_0)$

Multiplying the reduced pulsation ω_{R-T} by the factor a_A gives the x-axis ω_{R-TA}. A correction must also be made on the y-axis. $|E^*_{R-A}|$ is the reduced norm of the complex stiffness modulus (Equation (24)). It is 'reduced' because by multiplying ω_{R-TA} with $\Im_{\eta,R-TA}$, the influence of the factor b_A stays present. If we apply these operations for the specimen S2 at 15, 30 and 60 µm/m with their respective experimental coefficients a_A (1.463, 1.000 and 0.518) and b_A (0.947, 1.000 and 1.061), we obtain a single curve on the graph $|E^*_{R-A}|(\omega_{R-TA})$ (Figure 12). All the points overlap on the CMT at 30 µm/m for the specimen S2 validating the values calculated. This verification was also performed with the phase angle φ_{E^*}, which

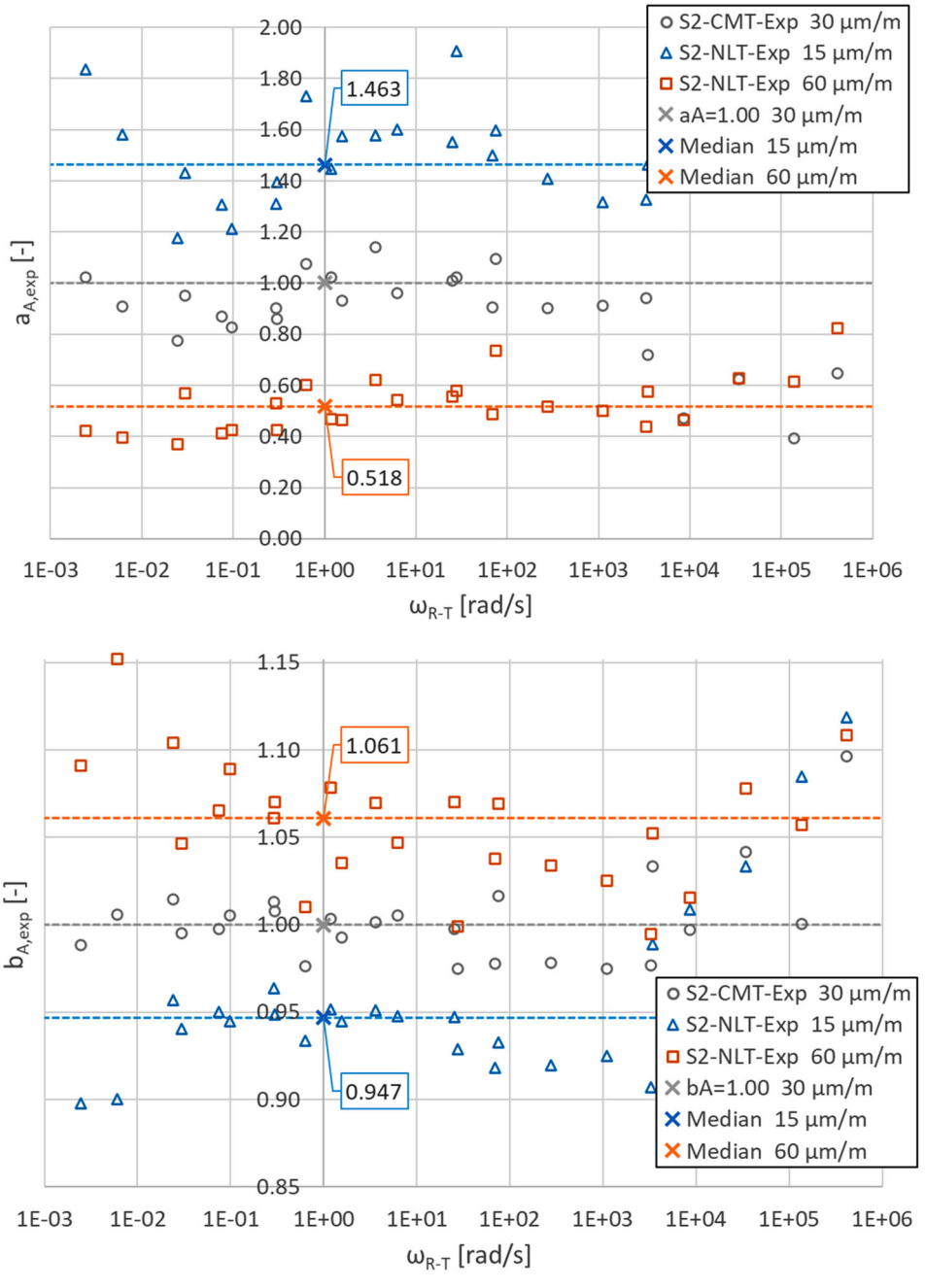

Figure 11. Graziani's asphalt concrete – Specimen S2 (CMT, 30 µm/m and NLT, 15/60 µm/m). Dispersion of the TASSP translation factors $a_{A,exp}$ (top) and $b_{A,exp}$ (bottom) according to the reduced pulsation ω_{R-T}. Plotting of experimental data and the median (dotted lines).

is correct.

$$|E^*_{R-A}| = \sqrt{\Re_E{}^2 + \left(\frac{\omega \cdot \Im_\eta}{b_A}\right)^2} \tag{24}$$

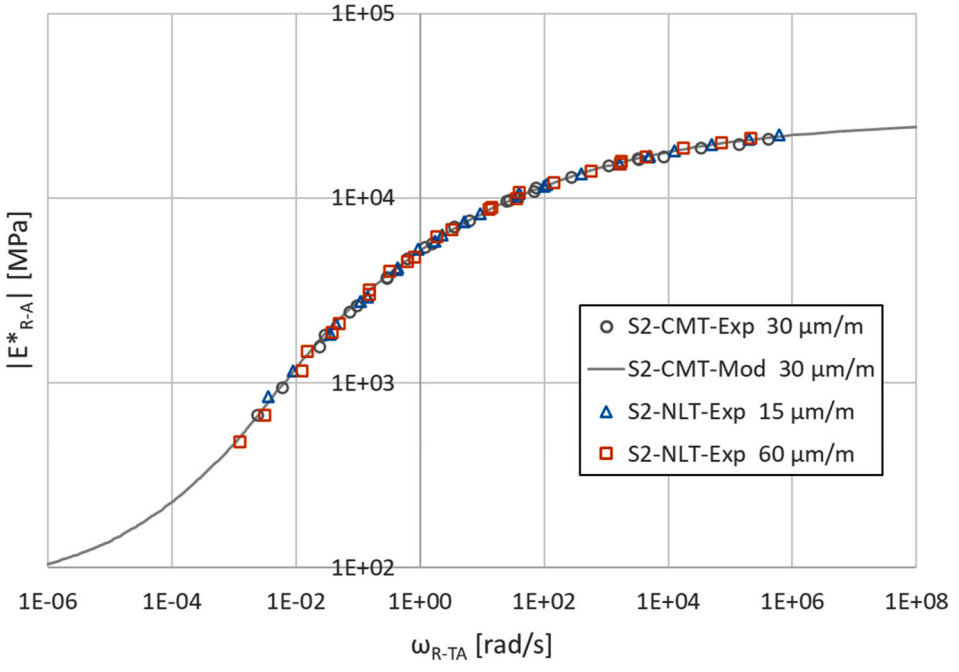

Figure 12. Graziani's asphalt concrete – Specimen S2 (CMT, 30 µm/m and NLT, 15/60 µm/m). Plotting of experimental data for the reduced norm of the complex stiffness modulus $|E^*_{R-A}|$ as a function of the reduced pulsation ω_{R-TA}. The CMT at $\varepsilon_{0,ref} = 30\mu m/m$ was modelled with the VENoL(T,ω) model.

4.5.3. Calibration of WLF-type equations

The average median values of $a_{A,exp}$ and $b_{A,exp}$ at 30 and 60 µm/m for the specimens S1 and S2 are plotted in a graph as a function of the strain amplitude ε_0 (Table 5, Figure 13). As with the Zeng et al. (2001)'s coefficient a_γ, we found the WLF equation appropriate to fit the variations of experimental values $a_{A,exp}$ and $b_{A,exp}$ according to ε_0 (Equations (25) and (26)). The use of these equations requires defining a reference amplitude $\varepsilon_{0,ref}$, which is 30 µm/m in this study. $C_{1,aA}$, $C_{2,aA}$ and $C_{1,bA}$, $C_{2,bA}$ are constants parameters (Table 6). The factors a_A and b_A are equal to 1.0 at $\varepsilon_{0,ref}$.

$$\log a_A(\varepsilon_0) = \frac{-C_{1,aA} \cdot (\varepsilon_0 - \varepsilon_{0,ref})}{C_{2,aA} + (\varepsilon_0 - \varepsilon_{0,ref})} \tag{25}$$

$$\log b_A(\varepsilon_0) = \frac{-C_{1,bA} \cdot (\varepsilon_0 - \varepsilon_{0,ref})}{C_{2,bA} + (\varepsilon_0 - \varepsilon_{0,ref})} \tag{26}$$

Table 5. Graziani's asphalt concrete – Specimens S1 and S2. Experimental values obtained for the TASSP translation factors $a_{A,exp}$ and $b_{A,exp}$.

	S1 (median)		S2 (median)		Average median	
Strain amplitude [µm/m]	$a_{A,exp}$	$b_{A,exp}$	$a_{A,exp}$	$b_{A,exp}$	$a_{A,exp}$	$b_{A,exp}$
15	1.526	0.942	1.463	0.947	1.495	0.945
30 (reference)	1.000	1.000	1.000	1.000	1.000	1.000
60	0.487	1.081	0.518	1.061	0.503	1.071

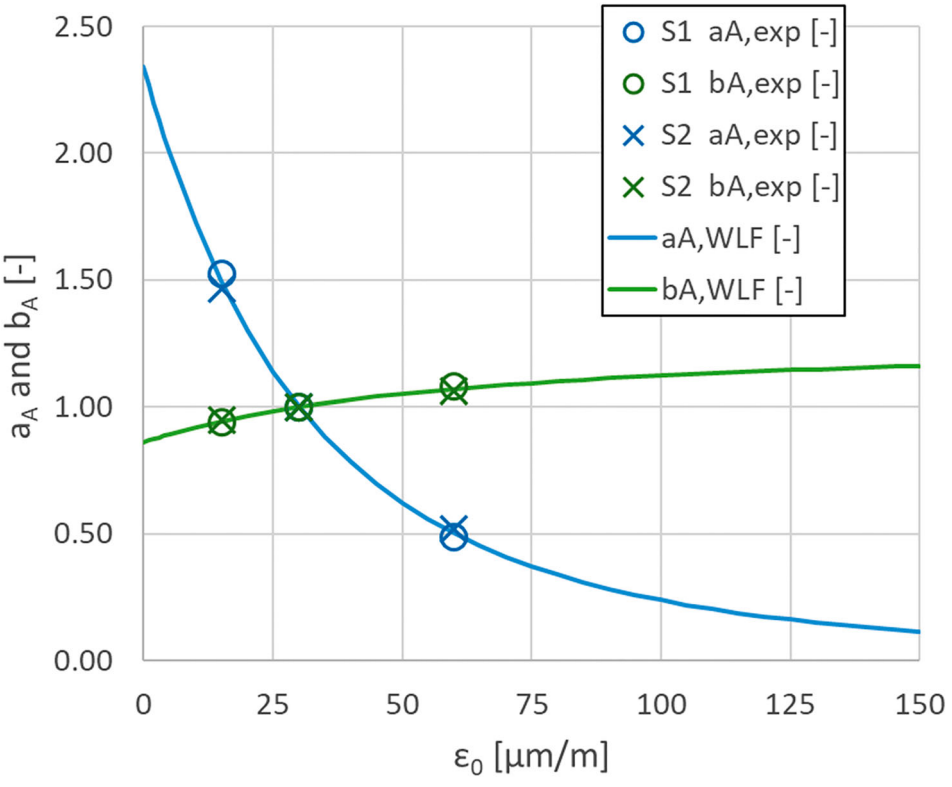

Figure 13. Graziani's asphalt concrete. Variation of the TASSP translation factors a_A and b_A according to the strain amplitude ε_0. Plotting of experimental factors and fit with two WLF-type equations.

Table 6. Graziani's asphalt concrete. Parameters of the WLF-type equations determining the evolution of the TASSP translation factors a_A and b_A.

Parameters	$a_{A,WLF}$	$b_{A,WLF}$
Reference amplitude [m/m]	$\varepsilon_{0,ref} = 3.00 \cdot 10^{-5}$	$\varepsilon_{0,ref} = 3.00 \cdot 10^{-5}$
Parameter 1 [-]	$C_{1,aA} = 3.200$	$C_{1,bA} = -0.108$
Parameter 2 [m/m]	$C_{2,aA} = 2.90 \cdot 10^{-4}$	$C_{2,bA} = 8.00 \cdot 10^{-5}$

4.6. Application of the TASSP

4.6.1. Prediction of nonlinear tests

The joint application of the VENoL model (Equations (15) and (16), Table 4) and TTASSP (Equations (9), (19), (20), (21), (25) and (26)) to the specimen S2 at the reference conditions $T_{ref} = 20°C$ and $\varepsilon_{0,ref} = 30\mu m/m$ allows us to obtain the prediction of NLTs results at different strain amplitudes (Figure 14). The results confirm the creation of the TASSP because the predictions are excellent at 15 and 60 µm/m. We can express a critical opinion concerning the prediction with high reduced pulsation at the level of the return of the curves in the Black space. The predicted curves do not pass perfectly through the experimental points at 15 and 60 µm/m (Figure 14, bottom). However, the number of experimental data at this level is too small to be able to conclude on the dispersion of experimental results or the imprecision of the modelling.

4.6.2. Prediction of strain amplitude rise tests

With the VENoL(T,ω,ϵ_0) model, some Strain Amplitude Rise Tests (SART) can be analytically modelled. It consists to increase the strain amplitude of 0 to 100 µm/m over the first 50 cycles. SARTs reproduce

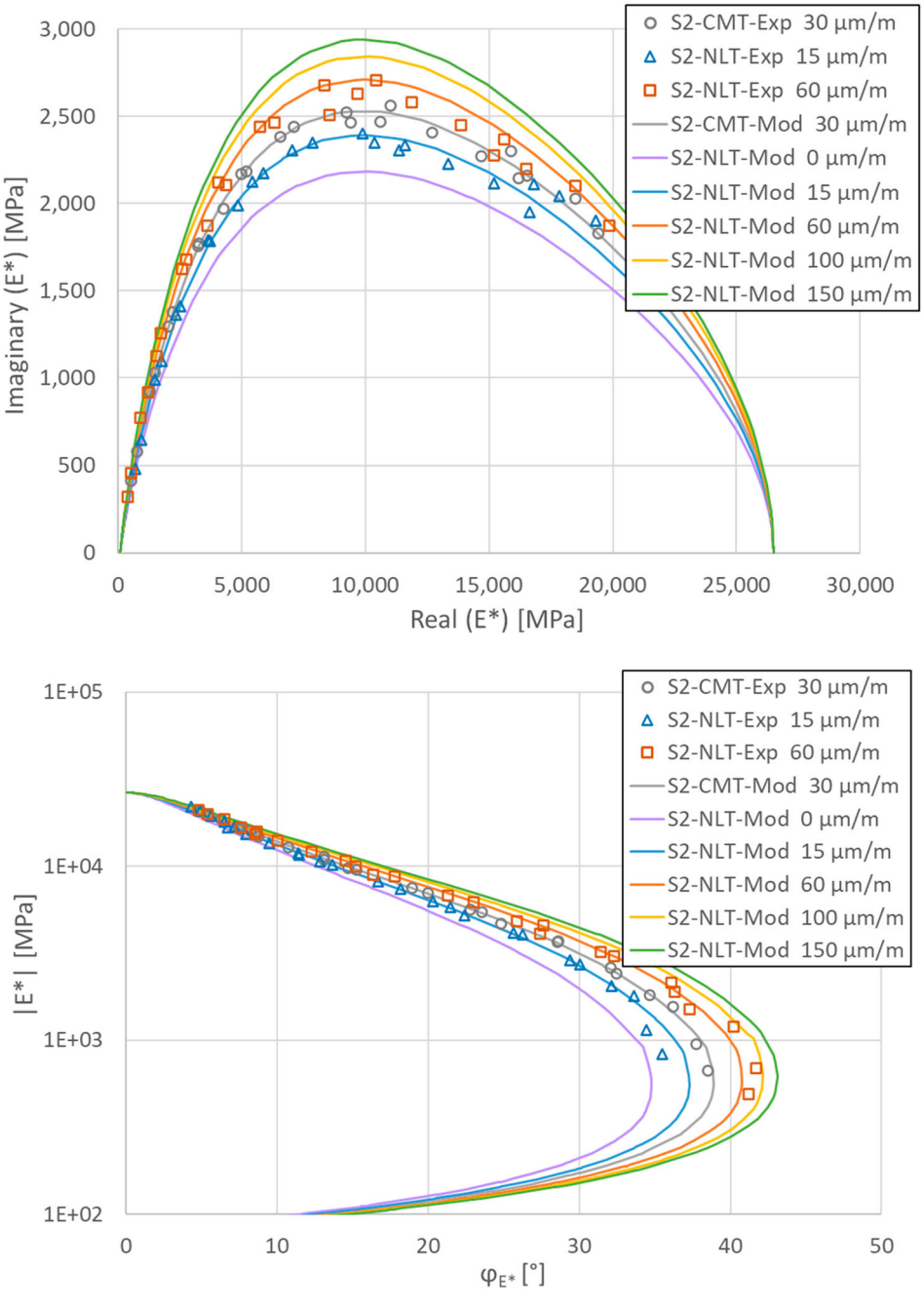

Figure 14. Graziani's asphalt concrete – Specimen S2 (CMT, 30 µm/m and NLTs, 15/60 µm/m). Plotting of experimental data and fit with the VENoL(T,ω,ϵ_0) model in the Cole-Cole (top) and Black (bottom) spaces.

the beginning of fatigue tests on bituminous mixtures, whose a strain amplitude rise is done to reach the desired amplitude. Over only 50 cycles, we consider that there are no effects of self-heating and thixotropy.

The SARTs are applied for different couples temperature-frequency with the VENoL model parameters determined for the specimen S1. Results are superimposed in the Cole–Cole space with CMTs and

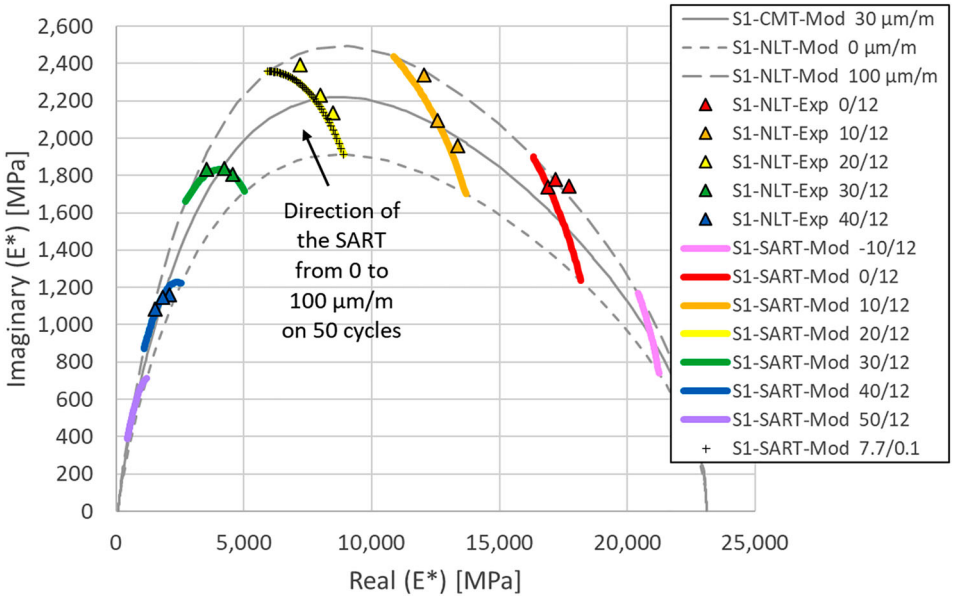

Figure 15. Graziani's asphalt concrete – Specimen S1 (CMT, 30 µm/m and NLTs, 15/60 µm/m). Overlay in the Cole-Cole space of modelled CMT (30 µm/m), modelled NLTs (0/100 µm/m) and modelled SARTs (0–100 µm/m over 50 cycles, for different temperatures at 12 Hz) with the use of the VENoL(T,ω,ϵ_0) model. To compare with the modelled SARTs, some experimental data targeted at the same temperatures and frequencies from CMT and NLTs at 15/30/60 µm/m are plotted. To verify the TTSP, one test is modelled at 20°C, 12 Hz and another one at 7.7°C, 0.1 Hz.

NLTs to see the nonlinearity direction for different couples temperature-frequency (Figure 15). Because the shift factor a_A decreases when amplitude increases, the nonlinearity direction follows a decrease in the reduced pulsation. With this type of test, nonlinearity effects on the norm of the complex stiffness modulus $|E^*|$ and the phase angle φ_{E^*} can be also observed at fixed temperatures and frequencies (Figure 16). $|E^*|$ decreases almost linearly when amplitude increases while φ_{E^*} increases almost linearly above 20 µm/m. The results tendencies are remarkably similar to the experimental works of Phan (Phan et al., 2017, especially figures 4, 5 and 11 from Phan's paper).

The LVE strain limits are deduced from the modelled SARTs by reading the strain amplitude for which the norm of the complex stiffness modulus decreased to 95% of its initial value. These limits $\varepsilon_{LVE\ limit}$ are plotted according to the reduced pulsation ω_{R-T} at the reference temperature of 20°C in Figure 17. For both specimens S1 and S2, the curves obtained are similar. The graph shows that this limit increases at high frequency and low temperatures, as is mentioned in the literature because the upper bound of the norm of the complex stiffness modulus is reached. As asphalt concretes also have a lower bound, the LVE strain limit increases at low frequency and high temperature. The inflexion point is located at the same reduced pulsation as the peak of the phase angle.

5. Discussion

5.1. Range of application of the VENoL model

The modelling of CMTs with the VENoL(T,ω) model has been confirmed for two different experimental data sources (Mangiafico and Graziani). They were obtained with asphalt concrete of different formulations (bitumen respectively of grade 35/50 and 70/100, continuous grading curve 0/14 mm and dense grading curve 0/11 mm), whose cylindrical specimen of different dimensions (D-75 x H-150 mm and D-94 x H-120 mm) were tested with DTC tests developed in two different countries (ENTPE, France and Università Politecnica delle Marche, Italia). For Mangiafico, CMTs were conducted at temperatures

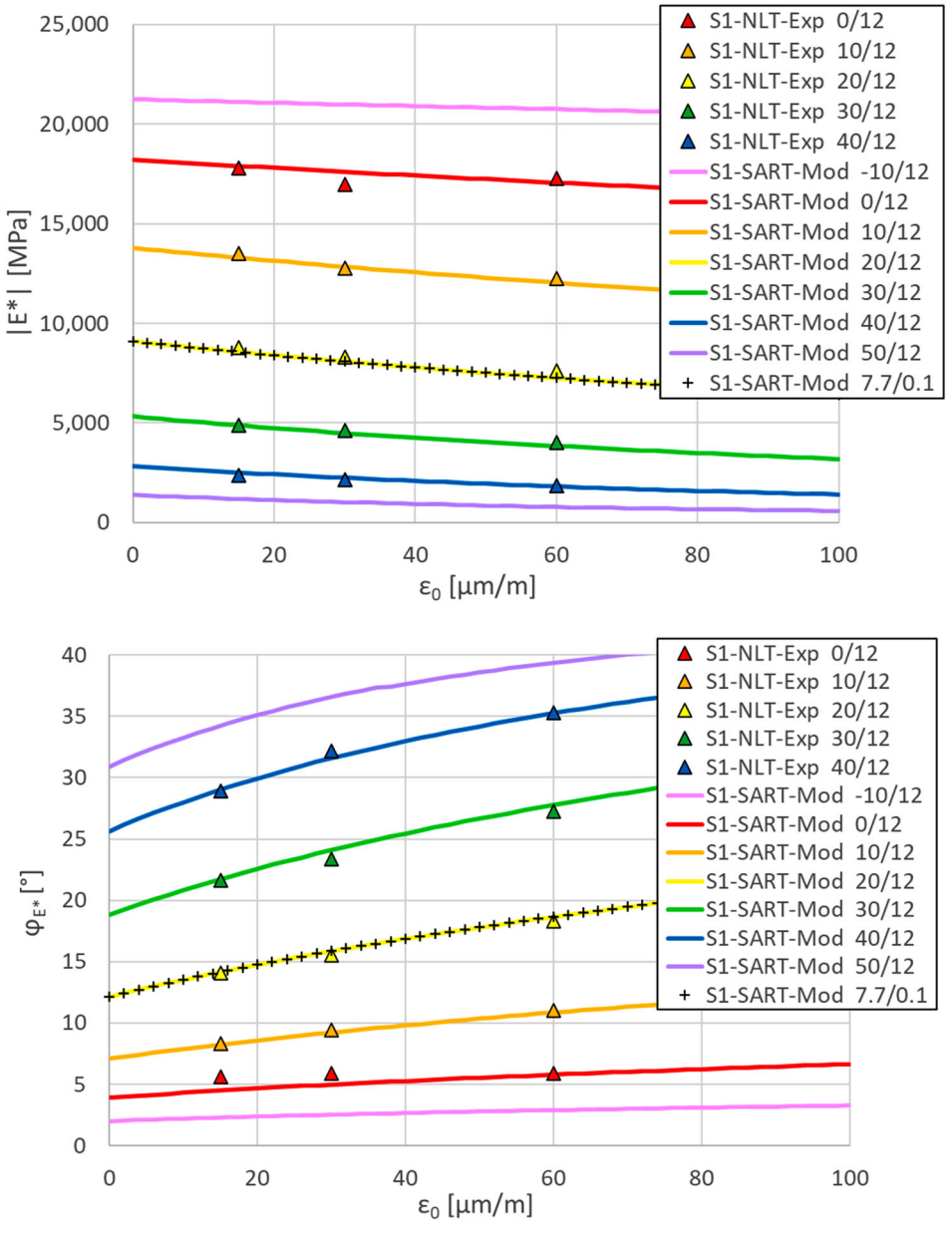

Figure 16. Graziani's asphalt concrete – Specimen S1 (CMT, 30 µm/m and NLTs, 15/60 µm/m). Evolution of the norm of the complex stiffness modulus $|E^*|$ (top) and the phase angle φ_{E^*} (bottom) during modelled SARTs (0–100 µm/m over 50 cycles, for different temperatures at 12 Hz) with the use of the VENoL(T,ω,ϵ_0) model. To compare with the modelled SARTs, some experimental data targeted at the same temperatures and frequencies from CMT and NLTs at 15/30/60 µm/m are plotted. To verify the TTSP, one test is modelled at 20°C, 12 Hz and another one at 7.7°C, 0.1 Hz.

ranging from −25 to 40°C and frequencies from 0.001 to 10 Hz. For Graziani, from 0°C to 40°C and 0.1 to 12 Hz. Likely, the VENoL model may be correct at a larger range of temperatures, such as −40 to 60°C for the same frequencies as previously.

The creation of the TASSP has been proven for two specimens, but only for one experimental data source (Graziani). In the literature, there are several papers about nonlinearity due to the strain amplitude, but to our knowledge, Graziani et al. are the only ones who have provided almost complete

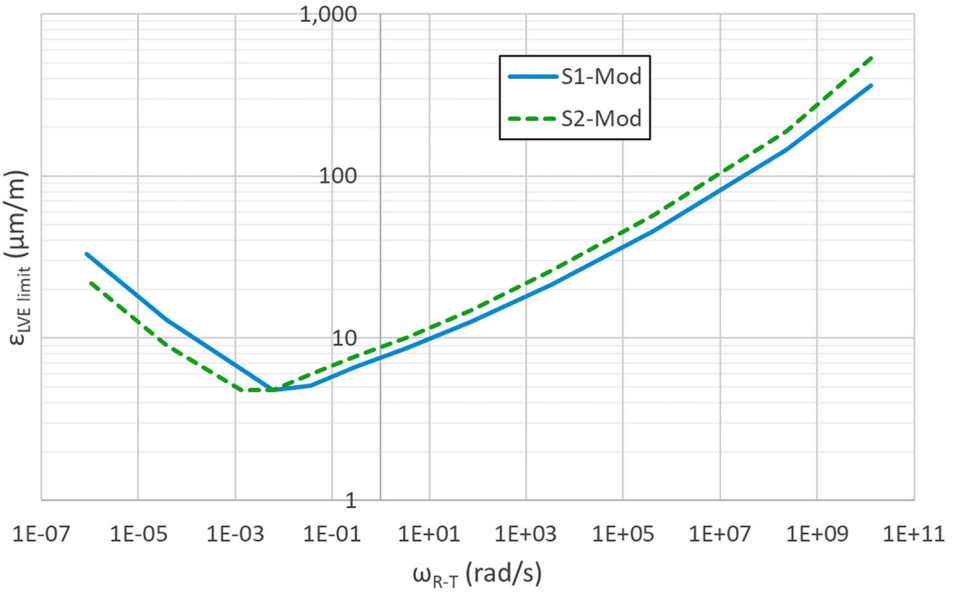

Figure 17. Graziani's asphalt concrete – Specimens S1 and S2. Evolution of the modelled LVE strain limit $\varepsilon_{LVE\ limit}$ according to the reduced pulsation ω_{R-T} at the reference temperature of 20°C.

curves in the Cole–Cole space for different strain amplitudes: 15, 30 and 60 µm/m. The TASSP applies for this small range. Nevertheless, the modelled decrease of the norm of the complex stiffness modulus as a function of strain amplitude in Figure 16 is in agreement with the experimental evolutions observed in the literature with larger ranges. Therefore, the TASSP may apply from 10 to 120 µm/m, and maybe higher. However, the modelling for $\omega_{R-T} \leq \omega_{R-T,tr}$ is only a prediction since the experimental points do not exceed the peak of the phase angle. Consequently, the TASSP will need to be verified with other data.

5.2. Comparison between the VENoL model and the models listed in the introduction

Figure 18 summarises the composition of the VENoL(T,ω,ϵ_0) model, which has been built for use with cyclic dynamic loadings. In total, twenty-two parameters (including two for the TTSP and four for the TASSP) are required to reproduce the NLVE behaviour.

Physical property	Symbol			Type of law	Nb param.
Stiffness component	$\Re_E$	$\omega_{R-TA} \leq \omega_{R-TA,tr}$		CY model	4
		$\omega_{R-TA} \geq \omega_{R-TA,tr}$		CY model	4
Viscosity component	$\Im_\eta$	$\omega_{R-TA} \leq \omega_{R-TA,tr}$		CY model	4
		$\omega_{R-TA} \geq \omega_{R-TA,tr}$		CY model	4
Influencing viscoelasticity:					
• signal pulsation ω					
• temperature T	TTSP	a_T		WLF law	2
• strain amplitude ε_0	TASSP	a_A	b_A	WLF law	2 + 2 = 4
	TTASSP	a_{TA}	b_A		

Figure 18. Summary of the VENoL(T,ω,ϵ_0) model.

The number of parameters of the VENoL model seems large at first sight since if we are interested in the LVE behaviour, VENoL(T,ω) model uses eighteen parameters (including two for the TTSP) whereas the 2S2P1D model requires only nine parameters (including two for the TTSP). However, the 2S2P1D model does not simulate perfectly at high temperature and low frequency, unlike the VENoL model. To make a fair comparison, the VENoL model must therefore be modified to the same level as the 2S2P1D model. From the equations of the stiffness and viscosity components $\Re_E$ and $\Im_\eta$ (Equations (15) and (16)), only those that are above the transition reduced pulsation $\omega_{R-T,tr}$ should be considered, and the parameter E_0, lower bound or low frequency stiffness limit, should be added to the stiffness component equation. Consequently, the VENoL model consists of eleven parameters (including two for the TTSP), which is only two more than the 2S2P1D model. In comparison, the generalised Maxwell and generalised Kelvin–Voigt models require at least thirty parameters to have an equivalent accuracy.

On the other hand, the number of parameters for the VENoL model can vary according to requirements. For example, if we desire to reproduce the behaviour of asphalt concrete only above the transition reduced pulsation $\omega_{R-T,tr}$, ten parameters (including two for the TTSP) are needed. With the generalised Kelvin–Voigt model, by adding a Kelvin–Voigt element, all the set of parameters must be redefined, which is not the case with the VENoL model.

In frequency analysis, modelling the NLVE behaviour with the VENoL(T,ω,ϵ_0) model is more accurate and complete than the nonlinear models listed in Section 1.2.2. Nevertheless, other rheological models could achieve equally good accuracy using the TASSP. Indeed, as for the TTSP, the TASSP is a principle independent of the structure of the VENoL model and could be applied to any rheological model as long as the real and imaginary parts can be dissociated. It should also be noted that the identification of the TASSP was made possible by the practicality of the structure of the VENoL model, since from the equations of stiffness and viscosity components $\Re_E$ and $\Im_\eta$ (Equations (15) and (16)), pulsation can be isolated to observe the effects of strain amplitude, which is difficult with rheological models from the literature.

This study also improves on the initial observations of Zeng et al. (2001). It confirms the existence of a shift factor at the frequency level as used in their nonlinear model. Thus, the shift factor a_A is assimilated to the shift factor a_γ from Zeng et al. Both factors decrease with increasing strain amplitude and are calibrated with a WLF-type equation. We also show here that if a_A applies to the frequency, it also applies to the viscosity as for the TTSP. However, the model of Zeng et al. is very imprecise regarding the phase angle. This problem is corrected in this paper by adding a vertical shift factor b_A on the imaginary part of the complex stiffness modulus. Another difference concerns the reference amplitude of the TASSP, which is left to the user's choice, whereas in Zeng et al. it is the origin of the strain amplitude (zero).

It is difficult to make a comparison between the TASSP and the nonlinear viscoelastic constitutive equations from Schapery (1969) since they were developed differently. Nevertheless, the shift factor a_A may be assimilated to a_ε and the correction factor b_A may be linked to the three nonlinear parameters h_e, h_1, h_2.

5.3. Relationship between dynamic and static behaviour

If we have to define a drawback of the VENoL model, it is currently only applicable to cyclic dynamic loading. It has not yet been studied for static loadings such as creep and relaxation tests. However, there may be bridges between the frequency and time analysis. For example, Equation (6) is already currently written as a function of time if only the real part is considered, but the stiffness and viscosity components as well as the TASSP are defined as a function of the pulsation. We recall that the pulsation is equal to the ratio of the angular velocity (maximum velocity of the signal) to the signal amplitude. Therefore, the pulsation of a sinusoidal strain can be written as the ratio of the strain rate amplitude $\dot{\varepsilon}_0$ by the strain amplitude ε_0 (Equation (27)). Furthermore, we believe that these maximum loading levels might influence the structural state of the bitumen (liquid/solid) which would control the stiffness and viscosity of the asphalt concrete. It is true that during a frequency cycle, the strain and the strain rate

vary between zero and their maximum, but for too high frequencies, the structural state of the asphalt might not have time to evolve and would remain dependent on the maximum loading levels. Thus, frequency analysis would have the advantage of isolating a structural state of the material according to a strain rate level and a strain level per frequency. Consequently, the stiffness and viscosity components, as well as the TASSP, might be defined more generally in terms of time parameters: strain and strain rate. However, principles should also be established to take into account the influence of loading and resting times. For example, if strain amplitude rise tests last too long, a duration effect will appear: the norm of the complex stiffness modulus decrease will accelerate (thixotropy?). For strain amplitude decay tests, a recovery effect will appear in addition: delayed recovery of complex modulus while the material structure rearranges itself. Therefore, the evolution of the complex modulus will be different between an amplitude rise test and a decay test, as shown in Mangiafico et al. (2018). Such an analysis would require a significant experimental campaign.

$$\omega = \frac{\dot{\varepsilon}_0}{\varepsilon_0} \tag{27}$$

5.4. Variations of a_A and b_A according to ε_0

In part 4.5.3, we have assumed that $a_{A,WLF}$ and $b_{A,WLF}$ took a finite value at 0 µm/m and were fitted with WLF-type equations. But some clues show us another possibility at low strain amplitude (between 0 and 20 µm/m). At high amplitude, they seem to move towards a limit.

Regarding Figure 13, above 30 µm/m, the factor $a_{A,WLF}$, fitted on the experimental data, seems to follow a trend equal to the inverse of the strain amplitude and normalised according to the reference strain amplitude. The number '2' is given to this second supposed trend of a_A (Equation (28), Figure 19). In fact, according to Equation (27), it is possible to obtain the same pulsation for different values of the strain amplitude and the strain rate amplitude. Indeed, to pass from 60 to 30 µm/m, the strain amplitude has to be divided by two; according to Equation (27), this is also equivalent to divide the strain rate amplitude by two to keep the pulsation constant. On the contrary, going from 15 to 30 µm/m leads to a doubling of the strain rate. Here we find the variations of the coefficient $a_{A,2}$. For a constant pulsation, the proportional evolution of the strain amplitude and the strain rate amplitude might explain the variations of the translation coefficient a_A. However, below 30 µm/m, the closer the amplitude is to 0 µm/m, the further $a_{A,WLF}$ seems to move away from $a_{A,2}$ (Figure 19). Indeed, by using Equation (28) for 15 and 60 µm/m, we should respectively find $a_{A,2}$ equal to 2.00 and 0.50 but, with the procedure of part 4.5, we had calculated the average median $a_{A,exp}$ equal to 1.495 and 0.503 for respectively 15 and 60 µm/m. This corresponds with 60 µm/m but not with 15 µm/m. Consequently, a second unidentified effect might occur in parallel of $a_{A,2}$ at very low amplitude to obtain $a_{A,WLF}$.

$$a_{A,2}(\varepsilon_0) = \frac{\varepsilon_{0,ref}}{\varepsilon_0} \tag{28}$$

Secondly, another discussion concerns the prediction of the shift factor b_A. In part 4.5.3, we have assumed that b_A took a finite value at 0 µm/m. Nevertheless, we think that $b_{A,2}$ might evolve very quickly approaching 0 µm/m to reach the value zero (Figure 19). Application of this law $b_{A,2}$ with $a_{A,WLF}$ would have strong modelling repercussions at low amplitude. The consequence would be an imaginary part equal to zero at 0 µm/m for each temperature-frequency pair. The real part would only depend on the temperature level (Figure 20). Approaching 0 µm/m, the norm of the complex stiffness modulus would increase until reaching the value of the real part, and the phase angle φ_{E^*} would decrease rapidly until reaching 0° for each couple temperature-frequency.

Nevertheless, despite some justifications, these trends about $a_{A,2}$ and $b_{A,2}$ at low strain amplitudes will remain hypotheses as long as this behaviour has not been confirmed or invalidated with other experimental data. Currently, it is preferable to consider the WLF-type equations of $a_{A,WLF}$ and $b_{A,WLF}$ to define the TASSP (Equations (25) and (26)).

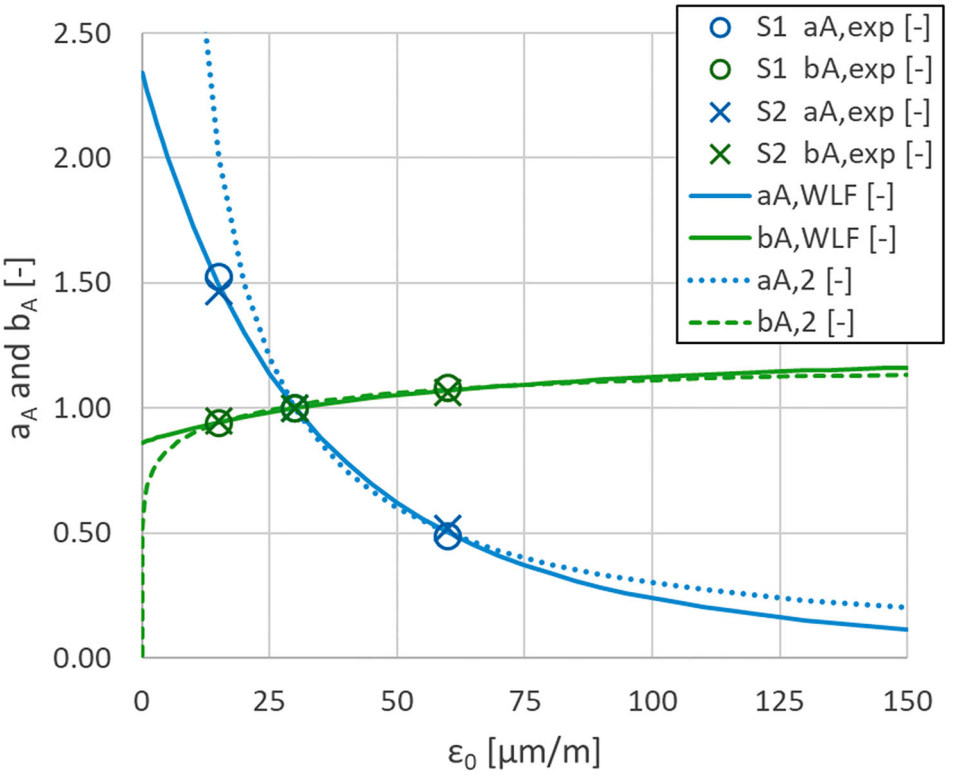

Figure 19. Graziani's asphalt concrete. Another assumed variation of the TASSP translation factors a_A and b_A according to the strain amplitude ε_0.

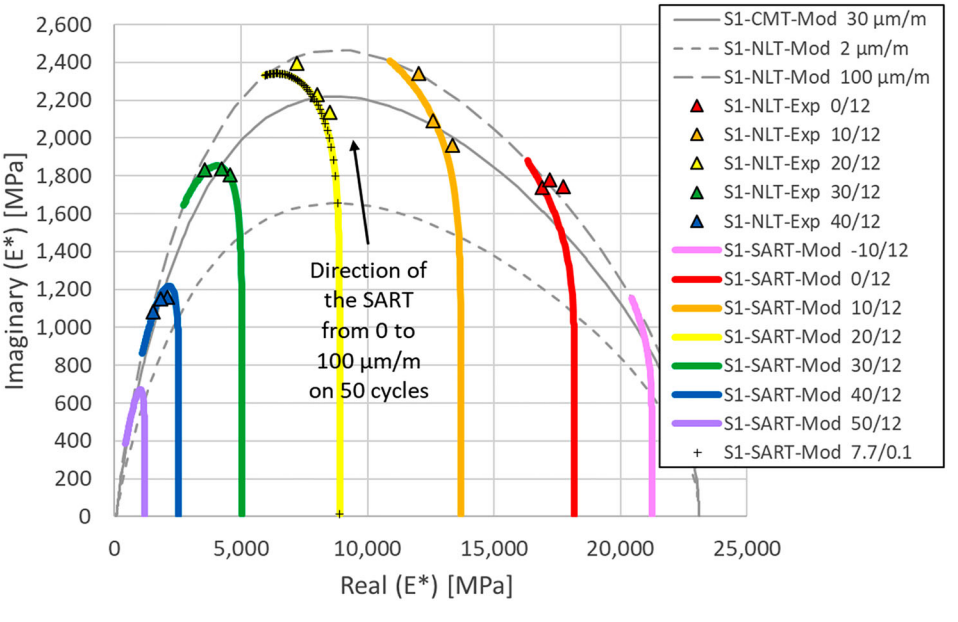

Figure 20. Graziani's asphalt concrete – Specimen S1 (CMT, 30 µm/m and NLTs, 15/60 µm/m). Overlay in the Cole-Cole space of modelled CMT (30 µm/m), modelled NLTs (2/100 µm/m) and modelled SARTs (0–100 µm/m over 50 cycles, for different temperatures at 12 Hz) with the supposed variations $a_{A,WLF}$ and $b_{A,2}$ from the TASSP. The cross marks of the modelled SART at 7.7°C and 0.1 Hz are plotted every 2 µm/m.

5.5. Physical meaning of a_A and b_A

In this study, we have shown that the shift factor a_A from the TASSP affects the same parameters (ω and $\Im_\eta$) as the shift factors a_T from the TTSP. We believe that these coefficients a_T and a_A might reflect the change of structural state of the material at the macroscopic level: fluidification (a_{TA} decreases) and solidification (a_{TA} increases). The coefficient b_A does not act in the same direction as the coefficient a_A. It might be considered a true nonlinear parameter because it changes the shape of the viscoelastic path. It might reflect different mechanisms within the microstructure between the influence of the strain amplitude and the temperature, which would impact the viscosity at the macroscopic level.

6. Conclusion

In this paper, an inventory of existing rheological models was first carried out to highlight the problems encountered in reproducing the LVE behaviour of asphalt concrete in dynamic analysis.

- The DRSMs require too many rheological elements to accurately reproduce the complex stiffness modulus at different temperatures and frequencies.
- The 2S2P1D model gives a correct simulation for only nine parameters, despite inaccurate modelling at high temperature and low frequency. However, fractional derivatives are difficult to implement in numerical simulations.

For these reasons, a different design of LVE model was proposed. It was given the name of 'VENoL model'.

- It is made up of two elements connected in parallel: a stiffness component $\Re_E$ related to the strain and a viscosity component $\Im_\eta$ related to the strain rate.
- These two components vary according to the pulsation at a reference temperature and are calibrated by using the Carreau–Yasuda model. The application of the TTSP makes the change from one temperature to another possible. Eighteen parameters are needed.
- The calibration of the parameters was confirmed for two different experimental data sources (Mangiafico and Graziani). The modelling of CMTs was accurate, in particular at high temperature and low frequency.
- The VENoL model can be reliably applied for a temperature range of -40 to 60°C and a frequency range of 0.001 to 12 Hz.
- Furthermore, based on a Kelvin–Voigt structure, the VENoL model can be easily implemented as a contact law in numerical simulations using DEM.

The second point concerns the addition of nonlinearity to the VENoL model, resulting from variations in strain amplitude. Research on NLVE modelling was first carried out in the literature.

- Three types of research were found: shift factors for the conversion from one stress or strain amplitude to another, nonlinear rheological models calibrated with the norm of the complex stiffness modulus and the phase angle, variation laws of the 2S2P1D model parameters according to strain amplitude. However, the models developed for the dynamic analysis are either incomplete or inaccurate.

To meet this need, a new principle was developed in this paper based on the same concept as the TTSP: the Time-Amplitude Semi-Superposition Principle (TASSP).

- It is defined by two translation factors a_A and b_A. As for the shift factor a_T from the TSSP, a_A influences the same parameters ω and $\Im_\eta$. However, b_A impacts only $\Im_\eta$. It is a true nonlinear parameter because it changes the shape of the viscoelastic path.

- When strain amplitude increases, a_A and b_A respectively decreases and increases towards a limit. At low strain amplitude (between 0 and 20 µm/m), their behaviour is not yet identified. We currently assume that they take a finite value at the origin 0 µm/m, but it is possible that b_A moves until zero.
- The TTSP and the TASSP add together to form the TTASSP: multiplying a_T by a_A gives the coefficient a_{TA}.
- The calibration of the TASSP has been verified for two specimens, but only for one experimental data source (Graziani). The joint application of the VENoL model and the TTASSP gives precise modelling of unmatched quality until now.
- The TASSP can be applied for small strain amplitudes from 10 to 120 µm/m.
- The existence of nonlinear shift factors due to various strain amplitudes confirms previous observations in the literature.

Acknowledgements

The authors warmly thank the authors Andrea Graziani, Fabrizio Cardone, Amedeo Virgili and Francesco Canestrari for kindly providing their experimental data presented in their paper (Graziani et al., 2019).

Disclosure statement

No potential conflict of interest was reported by the author(s).

Funding

The work presented in this paper was supported by the French institution Agence Nationale de la Recherche (ANR, eng: National Agency for Research) (ANR-MoveDVDC project, ref. ANR-17-CE22-0014-03).

References

Airey, G. D., Rahimzadeh, B., & Collop, A. C. (2004). Linear rheological behavior of bituminous paving materials. *Journal of Materials in Civil Engineering*, *16*(3), 212–220. https://doi.org/10.1061/(ASCE)0899-1561(2004)16:3(212)

Anderson, D. A., Christensen, D. W., Bahia, H. U., Dongre, R., Sharma, M. G., Antle, C. E., & Button, J. (1994). *Binder characterization and evaluation – Volume 3: Physical properties* (Strategic Highways Research Program, Rep. No. SHRP-A-369). Washington, DC: National Research Council.

Babadopulos, L., Orozco, G., Mangiafico, S., Sauzéat, C., & Di Benedetto, H. (2019). Influence of loading amplitude on viscoelastic properties of bitumen, mastic and bituminous mixtures. *Road Materials and Pavement Design*, *20*(S2), S780–S796. https://doi.org/10.1080/14680629.2019.1628428

Byron Bird, R., & Carreau, P. J. (1968). A nonlinear viscoelastic model for polymer solutions and melts—I. *Chemical Engineering Science*, *23*(5), 427–434. https://doi.org/10.1016/0009-2509(68)87018-6

Christensen, D. W., & Anderson, D. A. (1992). Interpretation of dynamic mechanical test data for paving grade asphalt cements. *Journal of the Association of Asphalt Paving Technologists*, *61*, 67–116.

Coulon, L. (2022). *Modelling the effect of ageing and fatigue on the residual behaviour of pavement materials* [Unpublished PhD thesis]. INSA de Strasbourg.

Coulon, L., Koval, G., Chazallon, C., & Roux, J.-N. (2021). Modeling of T/C complex stiffness modulus test and nonlinearity of asphalt concrete mixes. *Proceedings of the Rilem International Symposium on Bituminous Materials*, *27*(171), https://doi.org/10.1007/978-3-030-46455-4_171

Di Benedetto, H., Nguyen, Q. T., & Sauzéat, C. (2011). Nonlinearity, heating, fatigue and thixotropy during cyclic loading of asphalt mixtures. *Road Materials and Pavement Design*, *12*(1), 129–158. https://doi.org/10.1080/14680629.2011.9690356

Di Benedetto, H., Partl, M. N., Francken, L., & De La Roche Saint André, C. (2001). Stiffness testing for bituminous mixtures. Rilem Technical Committee 182-PEB: Performance testing and evaluation of bituminous materials. *Materials and Structures*, *34*(2), 66–70. https://doi.org/10.1007/BF02481553

Doubbaneh, E. (1995). *Comportement mécanique des enrobés bitumineux des « petites » aux « grandes » déformations* [PhD thesis]. INSA Lyon, 217 p. (in French)

Gauthier, G., Bodin, D., Chailleux, E., & Gallet, T. (2010). Non linearity in bituminous materials during cyclic tests. *Road Materials and Pavement Design*, *11*(S1), 379–410. https://doi.org/10.1080/14680629.2010.9690339

Graziani, A., Cardone, F., Virgili, A., & Canestrari, F. (2019). Linear viscoelastic characterisation of bituminous mixtures using random stress excitations. *Road Materials and Pavement Design*, *20*(S1), S390–S408. https://doi.org/10.1080/14680629.2019.1587494

Huet, C. (1963). *Étude, par une méthode d'impédance, du comportement viscoélastique des matériaux hydrocarbonés* [PhD thesis]. Faculté des Sciences de l'Université de Paris, 187 p. (in French)

Lesueur, D. (2009). The colloidal structure of bitumen: Consequences on the rheology and on the mechanisms of bitumen modification. *Advances in Colloid and Interface Science*, *145*(1-2), 42–82. https://doi.org/10.1016/j.cis.2008.08.011

Mangiafico, S. (2014). *Linear viscoelastic properties and fatigue of bituminous mixtures produced with Reclaimed Asphalt Pavement and corresponding binder blends* [PhD thesis]. ENTPE, 318 p.

Mangiafico, S., Babadopulos, L. F. A. L., Sauzéat, C., & Di Benedetto, H. (2018). Nonlinearity of bituminous mixtures. *Mechanics of Time-Dependent Materials*, *22*(1), 29–49. https://doi.org/10.1007/s11043-017-9350-3

Marasteanu, M. O. (1999). *Inter-conversions of the linear viscoelastic functions used for the rheological characterization of asphalt binders* [PhD thesis]. Pennsylvania State University.

Masson, J.-F., & Polomark, G. M. (2001). Bitumen microstructure by modulated differential scanning calorimetry. *Thermochimica Acta*, *374*(2), 105–114. https://doi.org/10.1016/S0040-6031(01)00478-6

Mouazen, M. (2011). *Évolution des propriétés rhéologiques des enrobés bitume, vers une loi vieillissement / viscosité* [Ph. D. thesis]. Mines ParisTech, 198 p. (in French).

Nguyen, Q. T., Di Benedetto, H., & Sauzéat, C. (2015). Linear and nonlinear viscoelastic behaviour of bituminous mixtures. *Materials and Structures*, *48*(7), 2339–2351. https://doi.org/10.1617/s11527-014-0316-5

Nguyen, Q. T., Nguyen, M. L., Di Benedetto, H., Sauzéat, C., Chailleux, E., & Hoang, T. T. N. (2019). Nonlinearity of bituminous materials for small amplitude cyclic loadings. *Road Materials and Pavement Design*, *20*(7), 1571–1585. https://doi.org/10.1080/14680629.2018.1465452

Olard, F. (2003). *Comportement thermomécanique des enrobés bitumineux à basses températures. Relations entre les propriétés du liant et de l'enrobé* [PhD thesis]. ENTPE, 228 p. (in French).

Phan, C. V., Di Benedetto, H., Sauzéat, C., Dayde, J., & Pouget, S. (2017). Quantification of different effects occurring during fatigue tests on bituminous mixtures. *Fatigue and Fracture of Engineering Materials and Structures*, 1–14. https://doi.org/10.1111/ffe.12646

Sayegh, G. (1965). *Variation des modules de quelques bitumes purs et bétons bitumineux* [PhD thesis]. Faculté des Sciences de l'Université de Paris (in French).

Schapery, R. A. (1969). On the characterization of nonlinear viscoelastic materials. *Polymer Engineering and Science*, *9*(4), 295–310. https://doi.org/10.1002/pen.760090410

Underwood, B. S., & Kim, Y. R. (2012). Comprehensive evaluation of small strain viscoelastic behavior of asphalt concrete. *Journal of Testing and Evaluation*, *40*(4), 622–632. https://doi.org/10.1520/JTE104521

Uzan, J., & Levenberg, E. (2007). Advanced testing and characterization of asphalt concrete materials in tension. *International Journal of Geomechanics*, *7*(2), 158–165. https://doi.org/10.1061/(ASCE)1532-3641(2007)7:2(158)

Williams, M. L., Landel, R. F., & Ferry, J. D. (1955). The temperature dependence of relaxation mechanisms in amorphous polymers and other glass-forming liquids. *Journal of the American Chemical Society*, *77*(14), 3701–3707. https://doi.org/10.1021/ja01619a008

Xu, Q., & Solaimanian, M. (2009). Modelling linear viscoelastic properties of asphalt concrete by the Huet-Sayegh model. *International Journal of Pavement Engineering*, *10*(6), 401–422. https://doi.org/10.1080/10298430802524784

Yasuda, K. (1979). *Investigation of the analogies between viscometric and linear viscoelastic properties of polystyrene fluids* [PhD thesis]. MIT, 587 p.

Zeng, M. (1997). *Nonlinear viscoelastic behaviour of asphalt concrete in stress relaxation* [PhD thesis]. University of Manitoba, 248 p.

Zeng, M., Bahia, H. U., Zhai, H., Anderson, M. R., & Turner, P. (2001). Rheological modeling of modified asphalt binders and mixtures. *Journal of the Association of Asphalt Paving Technologists*, *70*, 403–441.